Pulse-Splitting for Some Reaction-Diffusion Systems in One-Space Dimension

Theodore Kolokolnikov*, Michael J. Ward†, Juncheng Wei‡

Abstract

Pulse-splitting, or self-replication, behavior is studied for some two-component singularly-perturbed reaction-diffusion systems on a one-dimensional spatial domain. For the Gierer-Meinhardt model in the weak interaction regime, characterized by asymptotically small activator and inhibitor diffusivities, a numerical approach is used to verify the key bifurcation and spectral conditions of Ei, Nishiura, Ueda [Japan. J. Indust. Appl. Math., **18**, (2001)] that are believed to be essential for the occurrence of pulse-splitting in a reaction-diffusion system. The pulse-splitting that is observed here is edge-splitting, where only the spikes that are closest to the boundary are able to replicate. For the Gray-Scott model, it is shown numerically that there are two types of pulse-splitting behavior depending on the parameter regime: edge-splitting in the weak interaction regime, and a simultaneous splitting in the semi-strong interaction regime. For the semi-strong spike interaction regime, where only one of the solution components is localized, we construct several model reaction-diffusion systems where all of the pulse-splitting conditions of Ei, Nishiura, Ueda, can be verified analytically, yet no pulse-splitting is observed. These examples suggest that an extra condition, referred to here as the *multi-bump transition condition*, is also required for pulse-splitting behavior. This condition is in fact satisfied by the Gierer-Meinhardt and Gray-Scott systems in their pulse-splitting parameter regimes.

1 Introduction

In the singularly perturbed limit of small diffusivity, certain two-component reaction-diffusion systems in a one-dimensional spatial domain can support the existence of localized solutions, whereby one, or both, of the components of the system become localized around certain points in the domain. The resulting patterns are referred to either as spike-type, or pulse-type, patterns. Two such systems supporting these patterns are the Gray-Scott model (cf. [15]) and the Gierer-Meinhardt model (cf. [13]).

*Department of Mathematics, University of British Columbia, Vancouver, Canada V6T 1Z2
†Department of Mathematics, University of British Columbia, Vancouver, Canada V6T 1Z2 (corresponding author)
‡Department of Mathematics, Chinese University of Hong Kong, New Territories, Hong Kong

The Gierer-Meinhardt (GM) model (cf. [13]), and its extensions, have been widely used to model localization processes in nature including, patterns on sea-shells (cf. [25]), and cell differentiation and morphogenesis (cf. [24]). In dimensionless form, the GM model is a two-component system for an activator concentration a and an inhibitor concentration h, and can be written as (cf. [16])

$$a_t = \varepsilon^2 a_{xx} - a + \frac{a^p}{h^q}\,, \qquad -1 < x < 1\,, \quad t > 0\,, \tag{1.1a}$$

$$\tau h_t = D h_{xx} - h + \varepsilon^{-1}\frac{a^m}{h^s}\,, \qquad -1 < x < 1\,, \quad t > 0\,, \tag{1.1b}$$

$$a_x(\pm 1, t) = h_x(\pm 1, t) = 0\,; \qquad a(x,0) = a_0(x)\,, \qquad h(x,0) = h_0(x)\,. \tag{1.1c}$$

Here $0 < \varepsilon \ll 1$, $D > 0$, and $\tau > 0$, are assumed to be constants. The usual condition (cf. [13]) on the exponents (p, q, m, s) are that they satisfy

$$p > 1\,, \qquad q > 0\,, \qquad m > 1\,, \qquad s \geq 0\,, \qquad \text{with} \qquad \zeta \equiv \frac{qm}{(p-1)} - (s+1) > 0\,. \tag{1.2}$$

The Gray-Scott (GS) system, introduced in [15], models an irreversible reaction involving two reactants in a gel reactor, where the reactor is kept in contact with a reservoir of one of the two chemicals in the reaction. In the dimensionless variables of [28], this system is

$$v_t = \varepsilon^2 v_{xx} - v + A u v^2\,, \qquad -1 < x < 1\,, \quad t > 0\,, \tag{1.3a}$$

$$\tau u_t = D u_{xx} + (1-u) - u v^2\,, \qquad -1 < x < 1\,, \quad t > 0\,, \tag{1.3b}$$

$$v_x(\pm 1, t) = u_x(\pm 1, t) = 0\,; \qquad v(x,0) = v_0(x)\,, \qquad u(x,0) = u_0(x)\,. \tag{1.3c}$$

Here $A > 0$, $D > 0$, $\tau > 1$, and $\varepsilon \ll 1$.

For the GM and GS models, we refer to the parameter regime $D = O(1)$ and $\varepsilon \ll 1$ as the *semi-strong spike interaction regime*. In this regime, the two concentrations can be asymptotically decoupled in at least some asymptotic subinterval of $[-1, 1]$. For the GS model there are now many results available for the existence, stability, and dynamics, of spike patterns in the semi-strong interaction regime (cf. [4], [5], [6], [7], [9], [19], [20], [26], [27], [28]). Correspondingly, for the semi-strong regime of the GM model there has been a largely parallel theoretical analysis for the existence, stability, and dynamics, of spike patterns (cf. [8], [16], [17], [41], [42]).

Alternatively, the *weak interaction regime* for the GM and the GS models is defined by the parameter range $D = O(\varepsilon^2)$ and $\varepsilon \ll 1$. In this regime, both components are localized and highly coupled near certain points in the domain, and neighboring spikes interact by exponentially weak forces. A rigorous analysis for the existence and stability of spike patterns in this regime is difficult.

In the weak interaction regime, one of the most qualitatively interesting phenomena related to the GS and GM models is the possibility of self-replication, or pulse-splitting, behavior whereby new spikes are created dynamically from the splitting of certain spikes in a spike sequence. For the GS model, this behavior was first observed numerically in [34] in a two-dimensional square domain. The interest in studying pulse-splitting behavior was also motivated by its occurrence in actual physical experiments (cf. [21]). Initial studies for this behavior in a one-dimensional domain were given in [35], [36], and [37].

For the GS model, the pioneering studies of [31], [32], and [40], gave a theoretical explanation, based on a global bifurcation scenario, of the underlying mechanism responsible for pulse-splitting phenomena, and even chaotic behavior, in the weak interaction regime. For more general reaction-diffusion systems, specific bifurcation conditions that are believed to be essential for the occurrence of pulse-splitting behavior in a general setting are formulated in [11]. These key conditions, which play a central role in our study, are summarized below.

Alternatively, for the GM model in the weak interaction regime, pulse-splitting behavior can be observed from some of the numerical computations of [25]. However, no theoretical explanations are given there. Pulse-splitting behavior associated with a homoclinic stripe pattern for the GM model posed in a thin two-dimensional rectangular domain was computed in [10], but no bifurcation structure was analyzed. A preliminary numerical study of pulse-splitting for the GM model (1.1) using a moving-mesh method was done in [39]. An interesting example of pulse-splitting behavior for (1.1) was also given in [30] (see remark 6.2 page 257 of [30]).

The key conditions of [11] believed to be essential for pulse-splitting for a general reaction-diffusion system posed in $\mathbb{R}^1$, with bifurcation parameter σ, are summarized (roughly) as follows:

- **Lining-up Property:** Each k-spike equilibrium branch in terms of σ, must have a saddle-node, or fold-point, bifurcation. Moreover, the fold points for each of these branches of equilibria occur at the same bifurcation value $\sigma = \sigma_c$. This is the *lining-up property* of equilibria.

- **Spike Stability Condition:** For each fixed k, and for each of the two branches of equilibria that meet at the common saddle-node value, one branch is stable in the linearized sense, while the other branch is unstable.

- **Dimple Property:** In addition to the translation eigenfunction, the spectrum of the linearization of the equilibrium problem at each fold point location has a *dimple-shaped* eigenfunction Φ_d, associated with a zero eigenvalue, for one of the components of the system. By

definition, Φ_d is dimple-shaped if it exponentially localized and, for some $y_0 > 0$, has the property

$$\Phi_d(y) = \Phi_d(-y)\,; \quad \Phi_d(y) > 0\,, \quad \text{for} \quad y > y_0\,; \quad \Phi_d(y) < 0\,, \quad \text{for} \quad 0 \le y < y_0\,. \tag{1.4}$$

Thus, Φ_d has two positive lobes and one negative lobe (see Fig. 6 below).

- **Stability of the Background State:** The spatially homogeneous background state, away from the spike locations, is stable in the linearized sense.

Other more minor technical conditions given in [11] are that the eigenfunctions and spike solutions decay exponentially rapidly at infinity.

When the pulse-splitting conditions of [11] are satisfied, and when the bifurcation parameter is chosen to have a value slightly past the fold point value, pulse-splitting should occur from a single localized initial pulse. The *ghost* of the dimple eigenfunction at the fold point value still influences the system for values of the bifurcation parameter slightly past this critical value. Similar *ghost* effects in other bifurcation settings have been well-studied, including dynamical hysteresis loops (cf. [14]), and delayed bifurcation effects caused by slowly varying control parameters (cf. [12]).

The first goal of this paper is to give a detailed numerical study of pulse-splitting behavior in the GM model (1.1) in the weak interaction regime with $D = \varepsilon^2 D_0$, where D_0 is the bifurcation parameter. This problem is studied in §2. Our numerical computations identify a saddle-node bifurcation structure for a one-spike solution, and saddle-node bifurcation values D_{c0} for D_0 are computed for various exponent sets (p, q, m, s). In this weak interaction regime, where a and h are both localized, the existence of a saddle-node bifurcation value for D_0 for a one-spike equilibrium directly implies that the *lining-up property* of [11] will hold in a strict sense for k-spike equilibria. By studying the spectrum of the linearized problem, we verify numerically that the *spike stability condition* holds only for the parameter range $0 < \tau < \tau_H$. One branch is unconditionally unstable, whereas at each point on the other branch there can be a Hopf bifurcation if τ is large enough. The value τ_H ensures that the entire branch is stable to oscillatory instabilities for $0 < \tau < \tau_H$. Finally, we numerically verify that the *dimple property* holds, and that the background state is stable. Numerical experiments show that pulse-splitting does indeed occur.

In Fig. 1(a) we plot our bifurcation diagram for k-spike equilibria, which shows that a strict lining-up property holds for (1.1) when $(p, q, m, s) = (2, 1, 2, 0)$, and $D = \varepsilon^2 D_0$. For the GM model (1.1) with $(p, q, m, s) = (2, 1, 2, 0)$, the fold points are shown in §2 to coincide at the value $D = 7.171\varepsilon^2$ (see Fig. 1(a)). For this exponent set, the saddle-node value $D_{c0} = 7.171$ is consistent with a numerical result in [10]. In Fig. 1(b) we plot numerical trajectories of the maxima of a for

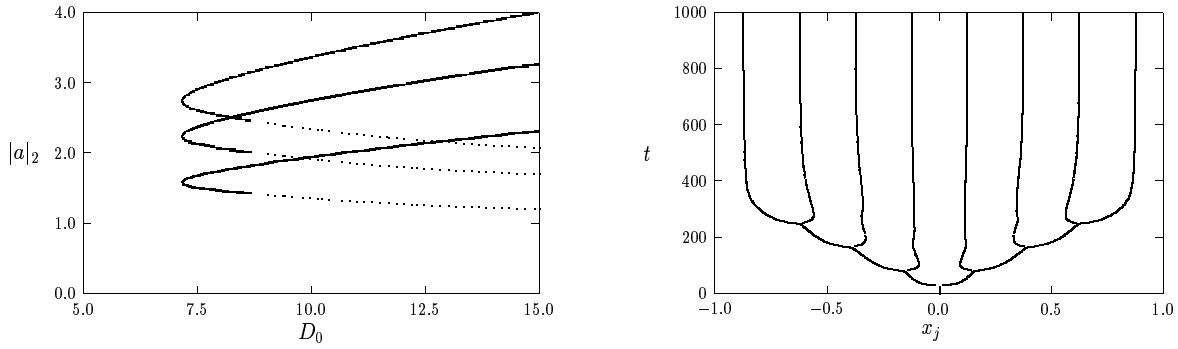

(a) $|a|_2$ for $k = 1, 2, 3$

(b) t versus x_j

Figure 1: Left figure: $|a|_2$, defined in (2.10), versus $D_0 \equiv D\varepsilon^{-2}$ for a k-spike solution to the GM model with $k = 1, 2, 3$ and $(p, q, m, s) = (2, 1, 2, 0)$. The fold point values increase with k. For the dotted portions of these curves there is a multi-bump structure in each spike core. Right figure: the trajectories $x_j(t)$ of the local maxima of a for $D = 6\varepsilon^2$, $\tau = 0.01$, and $\varepsilon = 0.02$.

(1.1), computed using the NAG software [29] for the value $D = 6\varepsilon^2$ with $\varepsilon = 0.02$. Indeed, pulse-splitting behavior is observed. The details of this, and similar, pulse-splitting computations are given in §2. For symmetric initial data, we observe from Fig. 1(b) that the type of pulse-splitting that occurs is *edge-splitting*, in which the spikes that are closest to the boundaries are the only ones that replicate. Edge-splitting behavior was first identified for the GS model in the weak interaction regime in [31], and a theoretical mechanism for this behavior is given in [11].

Our numerical computations, and investigations for other reaction-diffusion systems described below, suggests that in addition to the conditions of [11], a certain *multi-bump transition condition* must also hold for pulse-splitting to occur. For the solution component that is associated with the dimple eigenfunction, this multi-bump condition states that this component makes a transition between a one-bump profile on the stable branch to a two-bump profile at some point near the fold point on the unstable branch. Therefore, this condition implies that the spike profile develops an inflection point, at the location of its maximum, at some point along the the unstable branch. Numerically, we find that this multi-bump transition condition holds for the GM model (see Fig. 4 below). In the bifurcation diagram of Fig. 1(a), we have indicated by the dotted lines those portions of the bifurcation branches where the spike profile has a two-bump structure in each spike core.

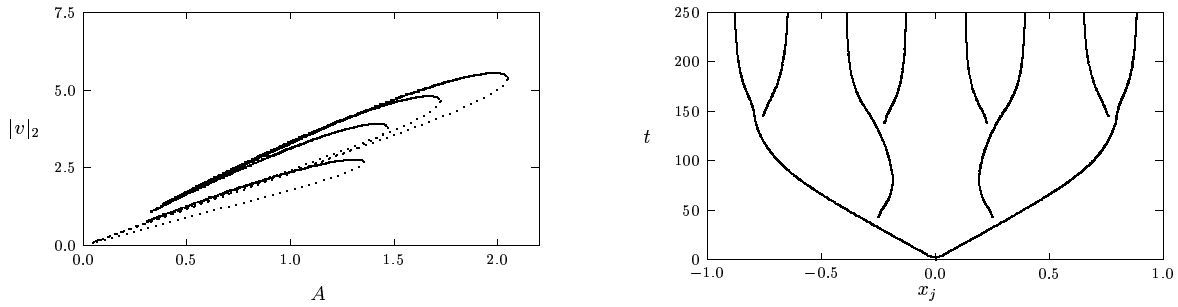

(a) $|v|_2$ versus A

(b) t versus x_j

Figure 2: Left figure: bifurcation diagram for the GS model for k-spike solutions with $\varepsilon = 0.01$, $D = 0.1$, and $k = 1, \ldots, 4$. The saddle-node values A_{pk} increase with k. Right figure: trajectories of the maxima of v showing pulse-splitting behavior when $\varepsilon = 0.01$, $D = 0.1$, $A = 2.4$, and $\tau = 2.0$.

Although pulse-splitting behavior does not occur for the GM model in the semi-strong interaction regime, this behavior has been found numerically for the semi-strong limit of the GS model of (1.3) when $A = O(1)$ (cf. [28], [9], [6], [5], [20]). In this particular semi-strong limit, which appears to be unique to the GS model, the u and v components can only be decoupled in the outer regions away from the core of each spike. However, these components are highly coupled near the spike core. In terms of a certain core problem identified in [28] for the infinite-line problem, k-spike equilibria for the finite-domain problem were constructed in [20]. Using a combination of analytical and numerical techniques, the pulse-splitting conditions of [11] described above were verified in a certain parameter regime. In §3, we briefly summarize these results. In Fig. 2(a) we plot an equilibrium bifurcation diagram for the GS model illustrating an approximate *lining-up property* of saddle-node equilibria in terms of the parameter A. The dotted lines in Fig. 2(a) indicate those portions of the branches of equilibria where v has a two-bump profile. In Fig. 2(b) we plot numerical trajectories of the maxima of v for a certain parameter set. Pulse-splitting behavior is indeed found to occur. From this figure, we notice that the pulse-splitting behavior is qualitatively very different from the edge-splitting behavior observed for the GM model, and also the GS model, in the weak interaction regime. For this semi-strong regime, spikes replicate roughly simultaneously and the final equilibrium state is qualitatively very different from that in the weak interaction regime. In §3 we numerically study the transition between these two distinct pulse-splitting regimes of the GS

model as a function of the diffusivity D.

Although the pulse-splitting conditions of [11] are clearly stated, it is generally intractable to verify *analytically* whether they are satisfied for a given reaction-diffusion system in the weak interaction regime. Moreover, for the special case of the GS model in the semi-strong pulse-splitting regime described above, where u and v are still coupled in the spike core, only a partial analytical verification of the pulse-splitting conditions was possible in [20].

Therefore, the second main goal of this paper is to try and formulate reaction-diffusion models in the semi-strong interaction limit where one can *analytically* verify all of the pulse-splitting conditions of [11]. This, hopefully, would lead to the existence of pulse-splitting behavior in a wide class of semi-strong reaction-diffusion systems of the form

$$u_t = \varepsilon^2 u_{xx} + f(u,v)\,, \qquad -1 < x < 1\,; \quad u_x = 0\,, \quad x = \pm 1\,, \tag{1.5a}$$

$$\tau v_t = D v_{xx} - v + \varepsilon^{-1} g(u,v)\,, \qquad -1 < x < 1\,; \quad v_x = 0\,, \quad x = \pm 1\,, \tag{1.5b}$$

where $D = O(1)$ as $\varepsilon \to 0$. For systems of the form (1.5), the components u and v can be asymptotically decoupled in the core of each spike, which makes it analytically tractable to construct equilibria and analyze their stability properties. For certain choices of f and g in (1.5), in §4 and §5 we introduce certain analytical techniques, similar to those in [19] and [41], in order to verify all of the pulse-splitting conditions of [11]. Since v in (1.5b) has a spatial variation over the entire interval $-1 < x < 1$, our analysis shows that the *lining-up property* of [11] now holds only in an approximate sense, similar to that shown in Fig. 2(a) for the GS model. The main difference between these models and the GS and GM models, where pulse-splitting is known to occur, is that the *multi-bump transition condition* described above is found not to hold. Numerical experiments for our model systems do not reveal pulse-splitting behavior. In addition to providing analytical techniques for verifying the conditions of [11], these examples strongly suggest that the *multi-bump transition condition* is also required for pulse-splitting to occur.

Finally, in §6 we close with a few open problems suggested by this study.

2 Pulse-Splitting: the GM Model with Weak Spike Interactions

In this section we study pulse-splitting phenomena for the GM model (1.1). This behavior is a consequence of the disappearance of certain homoclinic orbits when D in (1.1b) satisfies $D = O(\varepsilon^2)$ (cf. [10], [30], [39]). We show numerically that, when $D = O(\varepsilon^2)$, the criteria of [11] for pulse-splitting are satisfied and the *multi-bump transition condition* of §1 holds. In order to determine

the appropriate scaling of (1.1) for pulse-splitting behavior, we first recall an equilibrium result of [16] for the case where $D = O(1)$.

Proposition 2.1: (From [16]): *For $\varepsilon \to 0$ and $D = O(1)$, there is a unique one-spike equilibrium solution to (1.1), labeled by $a_e(x)$ and $h_e(x)$, which is given asymptotically by*

$$a_e(x) \sim H^{\gamma} w\left[\varepsilon^{-1} x\right], \qquad h_e(x) \sim \left(\frac{H}{\cosh\theta_0}\right)\cosh\left[\theta_0(1-|x|)\right], \tag{2.1}$$

where $\theta_0 \equiv D^{-1/2}$, and $\gamma \equiv q/(p-1)$. Here $w(y)$ is the unique positive solution to

$$w'' - w + w^p = 0\,, \quad -\infty < y < \infty\,; \quad w \to 0 \quad \text{as} \quad |y| \to \infty\,; \quad w'(0) = 0\,, \quad w(0) > 0\,, \tag{2.2a}$$

given by

$$w(y) = \left(\frac{p+1}{2}\right)^{1/(p-1)} \left(\cosh\left[\frac{(p-1)y}{2}\right]\right)^{-2/(p-1)}. \tag{2.2b}$$

In (2.1), the constant H satisfies $H^{\zeta} = 2\sqrt{D}\tanh\theta_0 \left(\int_{-\infty}^{\infty} w^m dy\right)^{-1}$, where ζ is defined in (1.2).

Although (2.1) is not valid when $D = O(\varepsilon^2)$, the formulae for a_e and h_e do suggest the appropriate re-scaling of (1.1) when $D = O(\varepsilon^2)$. Setting $D = O(\varepsilon^2)$ in (2.1), we get $h_e = O\left(\varepsilon^{1/\zeta}\right)$ and $a_e = O\left(\varepsilon^{\gamma/\zeta}\right)$. Hence, we introduce the new variables $\tilde{a}$, $\tilde{h}$, and D_0, defined by

$$h = \varepsilon^{1/\zeta}\tilde{h}\,, \qquad a = \varepsilon^{\gamma/\zeta}\tilde{a}\,, \qquad D = \varepsilon^2 D_0\,. \tag{2.3}$$

Substituting (2.3) into (1.1), we obtain the following re-scaled system on $-1 < x < 1$:

$$\tilde{a}_t = \varepsilon^2\tilde{a}_{xx} - \tilde{a} + \frac{\tilde{a}^p}{\tilde{h}^q}\,, \qquad \tau\tilde{h}_t = \varepsilon^2 D_0\tilde{h}_{xx} - \tilde{h} + \frac{\tilde{a}^m}{\tilde{h}^s}\,, \quad \text{with} \quad \tilde{a}_x = \tilde{h}_x = 0\,, \quad x = \pm 1\,. \tag{2.4}$$

When $D = O(1)$, the asymptotic analysis of [16], leading to Proposition 2.1, shows that $h_e \sim H$ and $a_e \sim H^{\gamma} w(y)$ within an $O(\varepsilon)$ inner region representing the core of the spike centered at $x = 0$. In contrast, when $D = O(\varepsilon^2)$, the inner problem for a one-spike equilibrium solution to (2.4) is such that both a and h are localized. In the inner region, we introduce the new variables

$$y = \varepsilon^{-1} x\,, \qquad u(y) = \tilde{a}(\varepsilon y)\,, \qquad v(y) = \tilde{h}(\varepsilon y)\,. \tag{2.5}$$

Substituting (2.5) into the equilibrium problem for (2.4), we obtain that u and v satisfy

$$u'' - u + u^p/v^q = 0\,, \qquad D_0 v'' - v + u^m/v^s = 0\,, \qquad 0 < y < \infty\,, \tag{2.6}$$

subject to the symmetry condition $v'(0) = u'(0) = 0$. For each fixed D_0, we look for solutions to (2.6) for which $u \to 0$ as $y \to \infty$, with v bounded as $y \to \infty$. We refer to such a solution of (2.6) as the homoclinic orbit.

Numerically, we find below that there are no such solutions to (2.6) when $0 < D_0 < D_{c0}$, where D_{c0} is some critical value. Qualitatively, the reason why these solutions fail to exist when D_0 is sufficiently small is because v then decreases too fast as $y \to \infty$. This rapid decrease in v as $y \to \infty$ when $D_0 \ll 1$ can allow the term u^p/v^q in (2.6) to grow as $y \to \infty$. This, then, precludes the existence of a homoclinic orbit. In [39], a very rough estimate of D_{c0} is obtained from an analysis of (2.6) in the tail region where $y \gg 1$. By assuming that u and v are small when $y \to \infty$, and by calculating the appropriate exponential tail behavior, it was shown in [39] that there is no solution to (2.6) when $D_0 < [q/(p-1)]^2$. However, this bound is not very close to the numerically computed value for D_{c0} given below.

To determination of D_{c0} and the homoclinic orbit can only be done numerically. We now describe our numerical procedure. It is convenient to introduce a parameter α defined by $\alpha = u(0)$, and to determine the bifurcation diagram in the form $D_0 = D_0(\alpha)$ from the numerical solution to (2.6). Since the solution branch α versus D_0 is found to be multi-valued, we must formulate an extended system of boundary value problems to compute these branches numerically (cf. [18]). To do so, we differentiate (2.6) with respect to α to obtain

$$u_\alpha'' - u_\alpha + \frac{pu^{p-1}}{v^q}u_\alpha - \frac{qu^p}{v^{q+1}}v_\alpha = 0\,, \qquad 0 < y < \infty\,, \tag{2.7a}$$

$$v_\alpha'' - \frac{1}{D}\left(v_\alpha - \frac{mu^{m-1}}{v^s}u_\alpha + \frac{su^m}{v^{s+1}}v_\alpha\right) = -\frac{D_0'}{D_0^2}\left(v - \frac{u^m}{v^s}\right)\,, \qquad 0 < y < \infty\,. \tag{2.7b}$$

Here $D_0' \equiv dD_0/d\alpha$. The extended system (2.6) and (2.7) can be written as a first order system with eight unknowns, with two additional auxiliary unknowns D_0 and D_0'. For numerical purposes one must compute on a large, but finite, domain $0 < y < L$. The extended system (2.6) and (2.7) is solved on this domain, subject to the ten boundary conditions

$$u(0) = \alpha\,, \quad u'(0) = 0\,, \quad u_\alpha(0) = 1\,, \quad u_\alpha'(0) = 0\,, \quad u(L) = 0\,, \quad u_\alpha(L) = 0\,, \tag{2.8a}$$

$$v'(0) = 0\,, \quad v_\alpha'(0) = 0\,, \quad v'(L) = 0\,, \quad v_\alpha'(L) = 0\,. \tag{2.8b}$$

The initial point on the bifurcation curve for D_0 large is chosen to be the shadow system solution, corresponding to $D_0 = \infty$, for which v is spatially homogeneous.

We remark that a direct computation of equilibrium bifurcation diagrams for (1.1) by automatic bifurcation software routines is nontrivial when ε is very small owing to severe, but localized,

gradients in the equilibrium solutions. This preliminary singular perturbation reduction, leading to (2.6)–(2.8), yields a bifurcation problem that is not numerically stiff.

The extended system (2.6)–(2.8) is solved for each value of α using the boundary value solver COLSYS [2]. In this way, we obtain the bifurcation curve $D_0 = D_0(\alpha)$. This curve is found to have a fold point, where $D_0'(\alpha) = 0$, at some value $\alpha = \alpha_c$. We label the critical value D_{c0} by $D_{c0} \equiv D_0(\alpha_c)$. In Table 1 we give numerical results for D_{c0} and α_c for five different exponent sets. In our numerical computations we chose a domain length $L = 15$. The results in Table 1 are independent of L for $L > 15$. Our result for D_{c0} for the exponent set $(p, q, m, s) = (2, 1, 2, 0)$ was found previously in [10] using a different approach. However, no actual bifurcation diagram was generated in [10]. The fourth column in Table 1 are the critical values D_{h0} where spatially periodic solutions bifurcate off of the spatially homogeneous equilibrium solution $a = \varepsilon^{\gamma/\zeta}$ and $h = \varepsilon^{1/\zeta}$. This issue is discussed below in §2.2.

(p, q, m, s)	D_{c0}	α_c	D_{h0}	τ_h
$(2, 1, 2, 0)$	7.171	1.580	5.828	1.36
$(2, 1, 3, 0)$	10.354	1.417	9.899	1.75
$(3, 2, 2, 0)$	3.905	1.615	2.914	0.65
$(3, 2, 3, 1)$	4.410	1.525	3.732	1.34
$(2, 2, 3, 3)$	33.7	2.276	14.93	7.80
$(4, 2, 2, 0)$	0.886	1.358	1.000	0.34

Table 1: Numerical values for the fold point location $D_{c0} = D_0(\alpha_c)$, where $D_0'(\alpha_c) = 0$. The fourth column are values of D_0 where spatially periodic solutions bifurcate off of the spatially homogeneous solution $a = \varepsilon^{\gamma/\zeta}$ and $h = \varepsilon^{1/\zeta}$. The last column are the smallest values of τ where a Hopf bifurcation occurs at the fold point.

For each of the exponent sets in Table 1, we find numerically that there are two homoclinic orbit solutions of (2.6) when $D > D_{c0}$, and none when $0 < D < D_{c0}$. Since, for $D > D_{c0}$, both u and v decay as $y \to \infty$, we can superimpose these functions to obtain two different k-spike equilibrium solutions to (1.1). The result is summarized as follows:

Proposition 2.2: *Let $\varepsilon \to 0$ and $D = \varepsilon^2 D_0$, and assume that $D_0 > D_{c0}$. Then, there are two k-spike equilibrium solutions to (1.1) given asymptotically by*

$$a_{e\pm}(x) \sim \sum_{j=1}^{k} \varepsilon^{\gamma/\zeta}\, u\left[\varepsilon^{-1}(x - x_j)\right], \qquad h_{e\pm}(x) \sim \sum_{j=1}^{k} \varepsilon^{1/\zeta}\, v\left[\varepsilon^{-1}(x - x_j)\right], \tag{2.9}$$

where $x_j = -1 + \frac{(2j-1)}{k}$, *for* $j = 1, \ldots, k$. *Here* $\gamma = q/(p-1)$, *and* ζ *is defined in (1.2).*

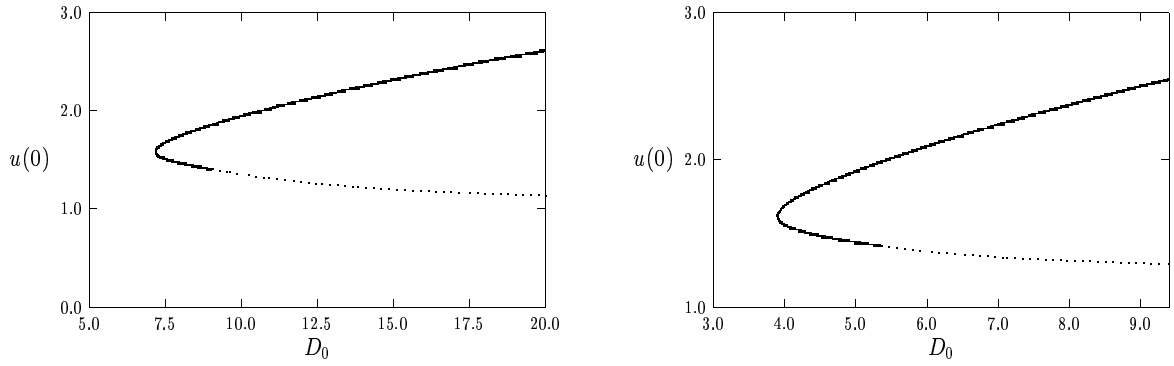

(a) $(p, q, m, s) = (2, 1, 2, 0)$ (b) $(p, q, m, s) = (3, 2, 2, 0)$

Figure 3: $\alpha = u(0)$ versus D_0 computed from (2.6) for two exponent sets. The left figure is for $(p, q, m, s) = (2, 1, 2, 0)$, while the right figure is for $(p, q, m, s) = (3, 2, 2, 0)$. The dotted portions of these curves are where the u profile has a two-bump structure.

Since $a_{e\pm}$ is exponentially small as $\varepsilon \to 0$ for $x \neq x_j$, we can calculate a norm of $a_{e\pm}$ as

$$|a|_2 \equiv \varepsilon^{-\gamma/\zeta} \left(\sum_{j=1}^{k} [a_{e\pm}(x_j)]^2 \right)^{1/2} \sim u(0)\sqrt{k} = \alpha\sqrt{k}\,. \tag{2.10}$$

With the curve $D_0 = D_0(\alpha)$ as computed from (2.6)–(2.8), we can then plot $|a|_2$ versus D_0 for a k-spike solution branch. Equation (2.10) clearly shows that a strict lining-up property of k-spike equilibria, as described in §1, holds for the GM model (1.1) when $D = O(\varepsilon^2)$. In Fig. 3 we plot $\alpha = u(0)$ versus D_0 for two different exponent sets. The corresponding bifurcation diagram of $|a|_2$ versus D_0 for the exponent set $(p, q, m, s) = (2, 1, 2, 0)$ was shown in Fig. 1(a). For each of the exponent sets of Table 1, we have verified numerically that there is a topologically similar bifurcation diagram of α versus D_0, and that the *multi-bump transition condition* of §1 holds not far from the fold point.

Although it is not analytically possible to determine D_{c0} for arbitrary exponent sets (p, q, m, s), it is simple to show that $D_{c0} < 1$ for any exponent set satisfying $p - q = m - s > 1$. For such a set, we readily see that there is a solution to (2.6) with $D_0 = 1$ given by $v = u = f$, where $f(y)$ is

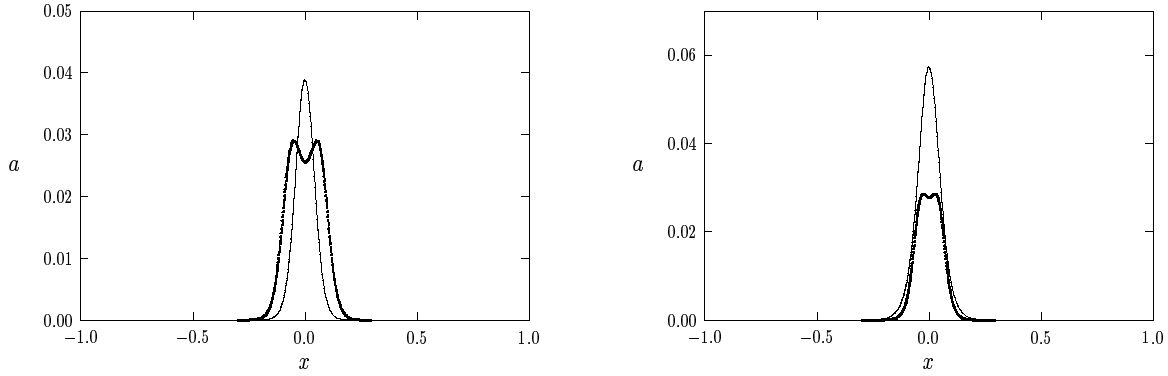

(a) $(p, q, m, s) = (2, 1, 2, 0)$ (b) $(p, q, m, s) = (3, 2, 2, 0)$

Figure 4: Plots of $a_{e\pm}$ for $\varepsilon = 0.02$. Left figure: a_{e+} (solid curve) for $D_0 = 9.83$ and a_{e-} (heavy solid curve) for $D_0 = 10.22$, when $(p, q, m, s) = (2, 1, 2, 0)$. Right figure: a_{e+} (solid curve) for $D_0 = 5.46$ and a_{e-} (heavy solid curve) for $D_0 = 5.68$, when $(p, q, m, s) = (3, 2, 2, 0)$.

the homoclinic solution satisfying

$$f'' - f + f^{p-q} = 0\,. \tag{2.11}$$

Therefore, since a solution to (2.6) exists when $D_0 = 1$, we must have $D_{c0} < 1$. The exponent set $(4, 2, 2, 0)$ in Table 1 is an example of such a set, where we found that $D_{c0} = 0.886 < 1$.

To illustrate the two-bump structure on much of the lower portion of the bifurcation curve, in Fig. 4 we plot $a_{e\pm}$, given in (2.9), for a one-spike solution with $\varepsilon = 0.02$. The plots are done for two exponent sets and for values of D_0 relatively close to the fold point. For each set, we plot a_{e+} and a_{e-} at roughly the same value of D_0. The two-bump behavior of a_{e-} is clear from this figure.

For the special exponent set $(2, 1, 2, 0)$, the existence of multi-bump solutions for (2.6) in the limit $D_0 \gg 1$ was established in [3]. The approach of [3] is also applicable to other exponent sets. However, for the special class of exponent sets $(p, q, m, s) = (p, q, p + 1, q + 1)$, we now show that the multi-bump behavior is readily seen through a certain conserved quantity. For this class of exponent sets, we assume that $q > p - 1$ so that $\zeta > 0$ in (1.2). We multiply the u and v equations in (2.6) by u' and $qv'/(p + 1)$, respectively. Subtracting the resulting equations, and integrating,

we then use $v \to 0$ and $u \to 0$ as $y \to \infty$ to obtain the first integral

$$u'^2 = u^2 - \frac{2}{p+1}\frac{u^{p+1}}{v^q} + \frac{2q}{p+1}\left(\frac{D_0 v'^2}{2} - \frac{v^2}{2}\right) . \tag{2.12}$$

Setting $y = 0$ where $u' = v' = 0$, and labeling $u_0 = u(0)$ and $v_0 = v(0)$, we obtain

$$u_0^2 = \frac{2u_0^{p+1}}{(p+1)v_0^q} + \frac{qv_0^2}{p+1} . \tag{2.13}$$

A multi-bump solution for u is formed when $u''(0) = 0$, or equivalently when $u_0 = u_0^p/v_0^q$. This equation, combined with (2.13), can be solved to yield the critical values

$$u_{0m} = \left(\frac{p-1}{q}\right)^{q/[2(p-q-1)]} , \qquad v_{0m} = \left(\frac{p-1}{q}\right)^{(p-1)/[2(p-q-1)]} . \tag{2.14}$$

It is also easy to see that $u''(0) = 0$ corresponds to the point where $dv_0/du_0 = 0$. Moreover, a simple calculation shows that the condition $v''(0) = 0$ corresponds to the point where $du_0/dv_0 = 0$. The values of u_0 and v_0 at this point are

$$u_{0*} = \left(\frac{p+1}{q+2}\right)^{(q+2)/[2(p-q-1)]} , \qquad v_{0*} = \left(\frac{p+1}{q+2}\right)^{(p+1)/[2(p-q-1)]} . \tag{2.15}$$

To illustrate this result, in Fig. 5(a) we plot u_0 versus v_0 for the exponent $(2, 2, 3, 3)$. For this set, (2.13) is a quadratic equation for v_0^2, which is readily solved. However, (2.13) does not directly yield a bifurcation diagram of u_0 versus D_0. By using COLSYS (cf. [2]), this diagram is shown in Fig. 5(b), where we have computed the critical value $D_{c0} = 33.83$. The dotted portions of the curves in Fig. 5 correspond to the region where $u''(0) > 0$, so that u has a multi-bump structure. We remark that the lower branch in Fig. 5 is locally flat at $u(0) = u_{0*} = 16/9$, which occurs at a value of D_0 that is beyond the range shown in Fig. 5(b).

2.1 The Stability of Solutions in the Pulse-Splitting Regime

Since u and v are exponentially localized, the stability of a k-spike solution can be inferred from the stability properties of a one-spike solution. To determine the stability of a one-spike solution, we write

$$a = \varepsilon^{\gamma/\zeta}\left[u(\varepsilon^{-1}x) + e^{\lambda t}\Phi(\varepsilon^{-1}x)\right] , \qquad h = \varepsilon^{1/\zeta}\left[v(\varepsilon^{-1}x) + e^{\lambda t}\eta(\varepsilon^{-1}x)\right] . \tag{2.16}$$

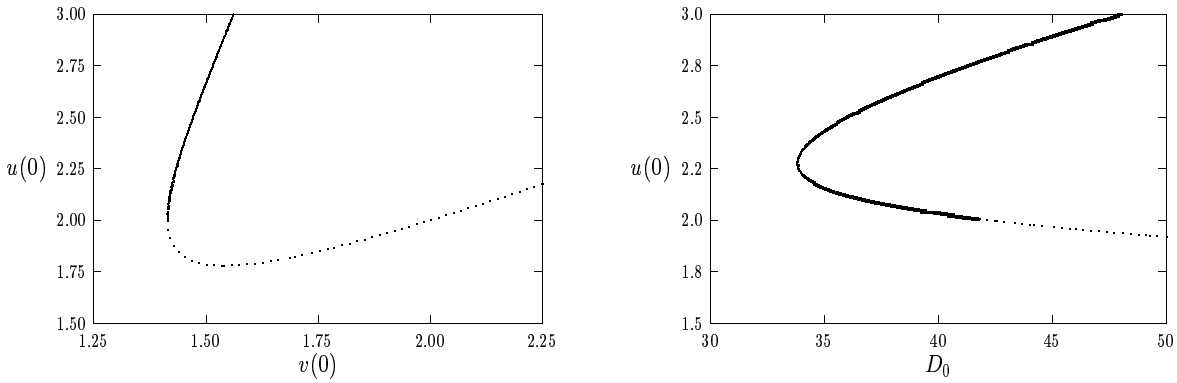

(a) $u(0)$ versus $v(0)$

(b) $u(0)$ versus D_0

Figure 5: Left figure: $u(0)$ versus $v(0)$ for the exponent set $(2,2,3,3)$. Right figure: $u(0)$ versus D_0 for the same exponent set. The portions of these curves where u has a multi-bump structure is indicated by the dotted lines.

Substituting (2.16) into (1.1), we obtain upon linearizing that $\Phi(y)$ and $\eta(y)$ satisfy

$$\Phi'' - \Phi + \frac{pu^{p-1}}{v^q}\Phi - \frac{qu^p}{v^{q+1}}\eta = \lambda\Phi\,, \qquad -\infty < y < \infty\,, \tag{2.17a}$$

$$D_0\eta'' - \eta + \frac{mu^{m-1}}{v^s}\Phi - \frac{su^m}{v^{s+1}}\eta = \tau\lambda\eta\,, \qquad -\infty < y < \infty\,, \tag{2.17b}$$

with $\Phi \to 0$ and $\eta \to 0$ as $|y| \to \infty$. We assume that $D_0 \geq D_{c0}$ so that u and v exist. The translation mode $\Phi = u'(y)$ and $\eta = v'(y)$, which are odd functions, is always an eigenfunction of (2.17) corresponding to $\lambda = 0$. Next, we observe that at the fold point where $\alpha = \alpha_c$ and $D_0' = 0$, the functions u_α and v_α satisfying (2.7), are solutions of (2.17) with $\lambda = 0$. Therefore, when $\alpha = \alpha_c$, the pair $\Phi = u_\alpha$, $\eta = v_\alpha$, which are both even functions, is also an eigenfunction of (2.17) corresponding to $\lambda = 0$. When $\alpha = \alpha_c$, we define a normalized eigenfunction $\Phi_d(y)$ by

$$\Phi_d(y) = -c\,u_\alpha(y)\,, \qquad c \equiv \left(\int_{-\infty}^{\infty} [u_\alpha(y)]^2\,dy\right)^{-1/2}\,. \tag{2.18}$$

In Fig. 6 we plot the numerically computed Φ_d for the exponent sets $(p,q,m,s) = (2,1,2,0)$ and $(p,q,m,s) = (3,2,2,0)$. This eigenfunction indeed has a dimple shape as referred to in §1. For

each of the exponent sets of Table 1, we have verified numerically that there is a dimple-shaped eigenfunction Φ_d at the fold point, corresponding to a zero eigenvalue.

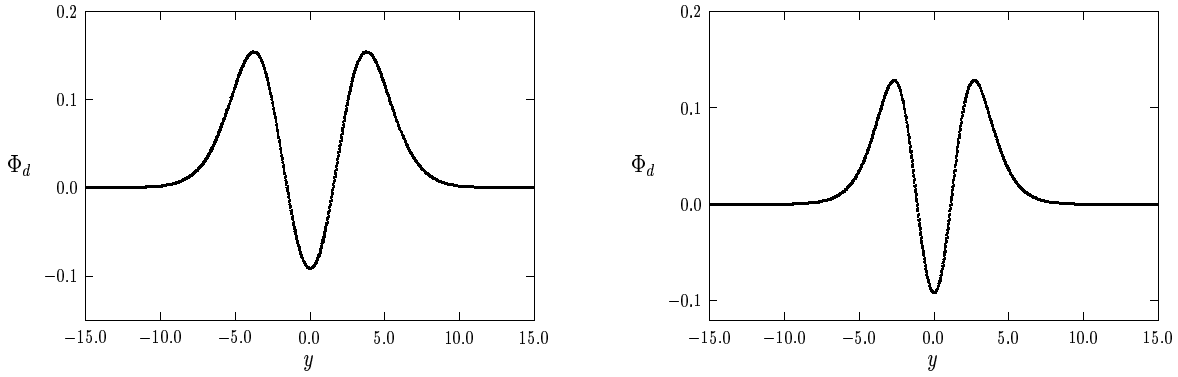

(a) $(p, q, m, s) = (2, 1, 2, 0)$ (b) $(p, q, m, s) = (3, 2, 2, 0)$

Figure 6: The dimple eigenfunction $\Phi_d(y)$, with $y = \varepsilon^{-1}x$, at the fold point for two different exponent sets.

Next, we compute the spectrum of (2.17) on both the upper and lower branches of the $u(0)$ versus D_0 curve. We discretize (2.17) on the interval $[0, L]$ using centered differences, ensuring that Φ and η are even functions. We label $y_1 = 0$, $y_N = L$, with $N > 1$, and we choose a meshsize $h = L/(N-1)$. In this way, the eigenvalues of (2.17) are approximated by the the discrete eigenvalues of the block matrix problem

$$\begin{pmatrix} \mathcal{M} - I + \Lambda_2 & -\Lambda_1 \\ \Lambda_3 & D_0\mathcal{M} - I - \Lambda_4 \end{pmatrix} \begin{pmatrix} \boldsymbol{\Phi} \\ \boldsymbol{\eta} \end{pmatrix} = \lambda \begin{pmatrix} I & 0 \\ 0 & \tau I \end{pmatrix} \begin{pmatrix} \boldsymbol{\Phi} \\ \boldsymbol{\eta} \end{pmatrix}. \tag{2.19a}$$

Here Λ_j, for $j = 1, \ldots, 4$, are $N \times N$ diagonal matrices with diagonal entries $(\Lambda_1)_{ii} = qu_i^p/v_i^{q+1}$, $(\Lambda_2)_{ii} = pu_i^{p-1}/v_i^q$, $(\Lambda_3)_{ii} = mu_i^{m-1}/v_i^s$, and $(\Lambda_2)_{ii} = su_i^m/v_i^{s+1}$, where $u_i = u(y_i)$ and $v_i = v(y_i)$.

The $N \times N$ matrix $\mathcal{M}$ is defined by

$$\mathcal{M} \equiv \frac{1}{h^2} \begin{pmatrix} -2 & 2 & 0 & \cdots & 0 & 0 & 0 \\ 1 & -2 & 1 & \ddots & \ddots & 0 & 0 \\ 0 & \ddots & \ddots & \ddots & \ddots & \ddots & 0 \\ \vdots & \ddots & \ddots & \ddots & \ddots & \ddots & \vdots \\ 0 & \ddots & \ddots & \ddots & \ddots & \ddots & 0 \\ 0 & 0 & \ddots & \ddots & 1 & -2 & 1 \\ 0 & 0 & 0 & \cdots & 0 & 2 & -2 \end{pmatrix} . \tag{2.19b}$$

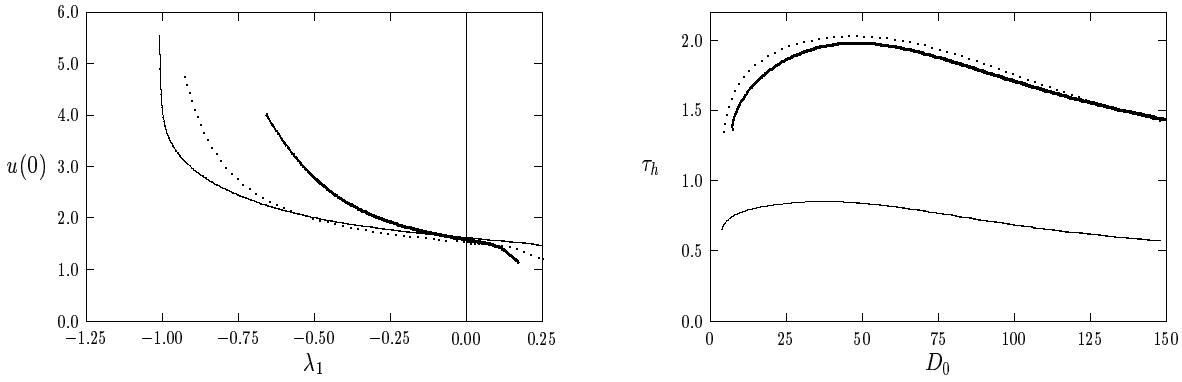

(a) $u(0)$ versus λ_1

(b) τ_h versus D_0

Figure 7: Left figure: $u(0)$ versus the maximum eigenvalue λ_1. Right figure: the Hopf bifurcation value τ_h versus D_0 on the upper branch. The heavy solid curves, solid curves, and dotted curves, correspond to the exponent sets $(2,1,2,0)$, $(3,2,2,0)$, and $(3,2,3,1)$, respectively.

The eigenvalues of the discrete problem (2.19) were computed using LAPACK [1] on a domain with $L = 15$ and $N = 200$. Increasing the number of meshpoints and the domain length did not change the results noticeably. For $\tau = 0.01$, and for three exponent sets (p,q,m,s), in Fig. 7(a) we plot $u(0)$ versus λ_1, where $\lambda_1 = \max(\mathrm{Re}(\lambda))$. For each of the exponent sets of Table 1, we find that $\lambda_1 < 0$ on the upper branch of the $u(0)$ versus D_0 curve, while $\lambda_1 > 0$ on the lower branch. Therefore, for τ sufficiently small, the upper branch is stable while the lower branch is unstable.

However, the upper branch of each $u(0)$ versus D_0 curve can be de-stabilized by increasing τ past some threshold τ_h, which depends on D_0. When τ is increased past this threshold, a pair of complex conjugate eigenvalues enters the unstable right half-plane, which leads to a Hopf bifurcation. The critical value τ_h is found by solving (2.19) numerically using LAPACK [1] together with Newton's method. For three exponent sets, plots of τ_h versus D_0 on the upper branch of the $u(0)$ versus D_0 curve are shown in Fig. 7(b). In the last column of Table 1 we give numerical values for τ_h at the fold point location.

In summary, we have exhibited numerically that the key properties for pulse-splitting of [11] hold for the GM model (1.1) when $D = O(\varepsilon^2)$ and $\varepsilon \ll 1$. Specifically, there is a strict lining-up property of k-spike equilibria, there is a dimple eigenfunction associated with a zero eigenvalue at the fold point, and there is a parameter range (i.e $\tau < \tau_h$) where each upper branch of equilibria is stable. Each lower branch is unstable for any $\tau \geq 0$. In addition, the *multi-bump transition condition* described in §1 is found to hold.

2.2 Numerical Experiments

We now display some time-dependent results computed from (1.1) using the NAG routine D03PCF (cf. [29]) using 1500 meshpoints and strict controls on the time-stepping. In each case, the initial condition was taken to be the one-spike profile given explicitly in Proposition 2.1.

Experiment 2.1: We first consider the exponent set $(p, q, m, s) = (2, 1, 2, 0)$ with $D = 6\varepsilon^2$, $\varepsilon = 0.02$, and $\tau = 0.01$. Notice from Table 1 that $D_0 < D_{c0} = 7.171$. In Fig. 1(b) of §1, we plot the trajectories $x_j(t)$ of the local maxima of a. In Fig. 8 we plot the solution at different times showing the pulse-splitting process, and the final equilibrium state that is obtained. Notice that, as predicted by the theory of [11], only the spikes that are furthest from the origin, referred to as edge spikes, are able to split. The final equilibrium state more closely resembles a periodic pattern rather than a pattern of isolated spikes.

Next, we consider the same exponent set $(p, q, m, s) = (2, 1, 2, 0)$ with $\varepsilon = 0.02$, but now we take $D_0 = 7.0$. In Fig. 9 we plot both the trajectories x_j of the local maxima of a and the final equilibrium state. Notice that for this value of D_0, which is closer to the saddle-node value $D_{c0} = 7.171$, the time-scale over which splitting occurs is significantly longer than in Fig. 1(b) (where $D_0 = 6$), and there are fewer pulse-splitting events. The increase in the time-scale is a result of being closer to the zero eigenvalue associated with the fold point.

Experiment 2.2: Next, we consider the exponent set $(p, q, m, s) = (3, 2, 2, 0)$ with $\varepsilon = 0.02$ and $\tau = 0.01$. From Table 1, the fold point value is $D_{c0} = 3.905$. In Fig. 10 we plot the spike trajectories

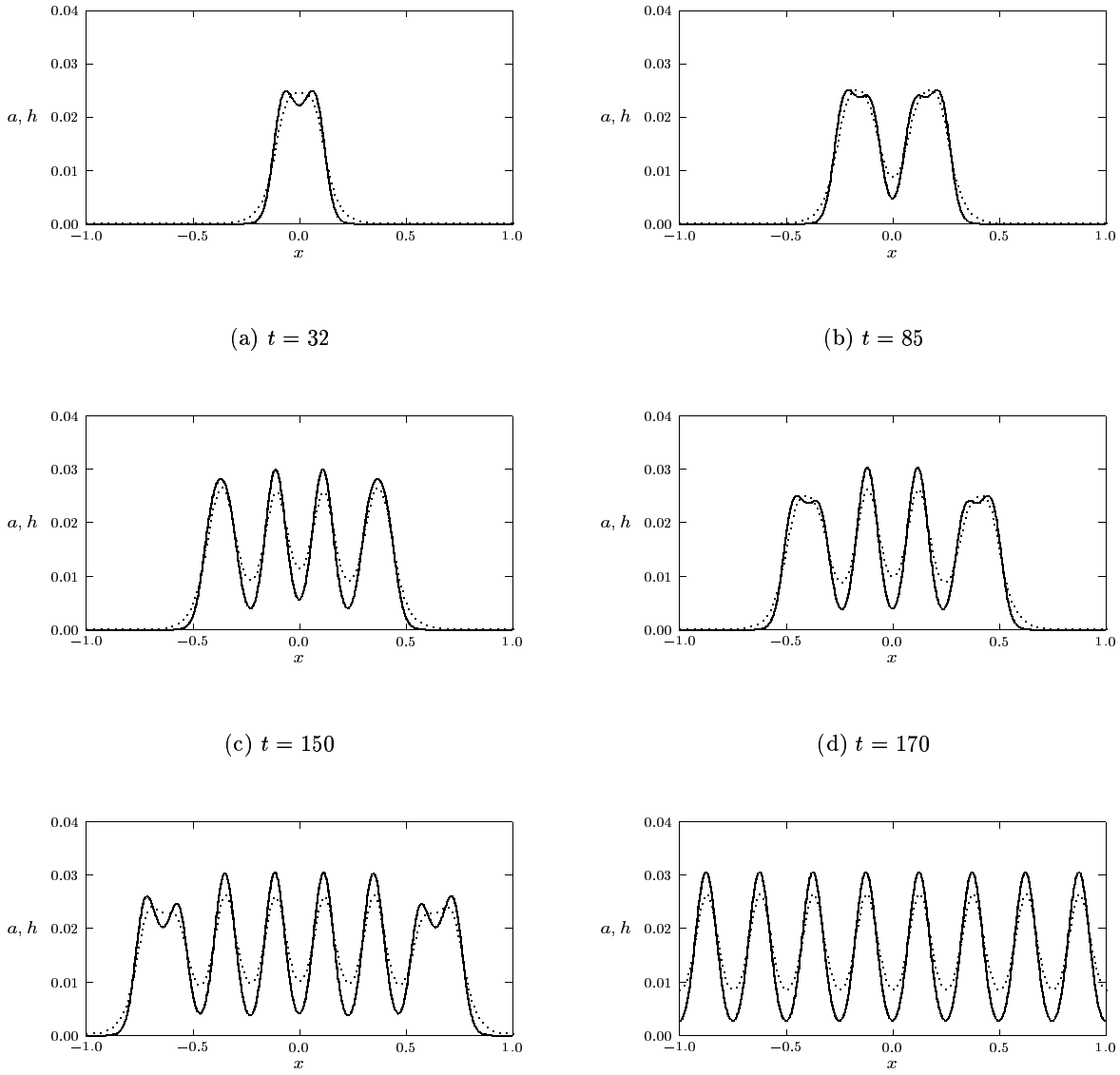

(a) $t = 32$

(b) $t = 85$

(c) $t = 150$

(d) $t = 170$

(e) $t = 260$

(f) $t = 800$

Figure 8: Experiment 2.1: $(p, q, m, s) = (2, 1, 2, 0)$, $D_0 = 6$, $\varepsilon = 0.02$, and $\tau = 0.01$. The heavy solid and dotted curves are a and h, respectively. The final plot when $t = 800$ is essentially the equilibrium solution.

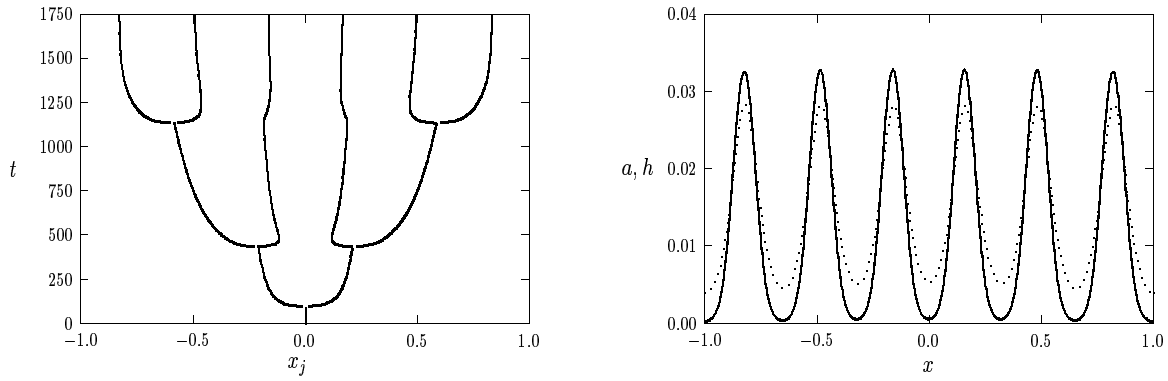

(a) t versus x_j

(b) a and h versus x.

Figure 9: Experiment 2.1: $(p, q, m, s) = (2, 1, 2, 0)$, $D_0 = 7$, $\varepsilon = 0.02$, and $\tau = 0.01$. Left figure: the spike trajectories t versus x_j. Right figure: the final equilibrium state for a (heavy solid curve) and h (dotted curve).

and the final equilibrium state for $D_0 = 3.5$ and for $D_0 = 3.8$, which is closer to the fold point value. Notice again that there are fewer pulse-splitting events when D_0 is closer to the fold point and that the time-scale is significantly longer.

In the limit $\varepsilon \ll 1$, and for values of D_0 slightly below the critical value D_{c0}, an asymptotic analysis similar to that given in the general framework of [11] can be applied to (1.1) to derive a set of differential equations for the motion of the centers of a collection of spikes. For repulsive spike interactions, it was shown in [11] that there exists a critical distance such that each spike does not start to split until the distance to the neighboring spikes exceeds this critical value. Since edge spikes reach this critical distance first (see §4.1 and Proposition 4.3 of [11]), the splitting process is referred to as edge-splitting. This type of splitting behavior is clearly shown in Fig. 9 and Fig. 10. However, the analysis in [11] is not applicable to the strong interaction regime when spikes are closely spaced, or when new spikes are born from a pulse-splitting event. In particular, from Fig. 8, Fig. 9, and Fig. 10, the final pattern that emerges after the splitting process has terminated more closely resembles a sinusoidal pattern than a sequence of isolated spikes. Therefore, the analysis in [11], which is based on an exponential decay of a and h between any two adjacent spikes, cannot be used to predict the number of maxima of a for the final equilibrium pattern.

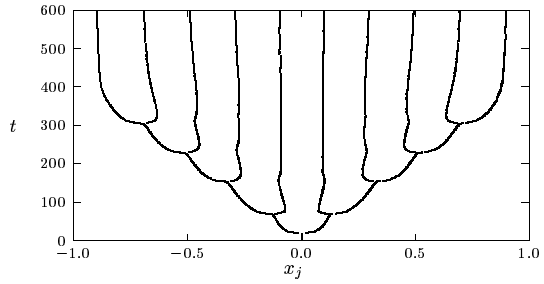

(a) t versus x_j: $D_0 = 3.5$

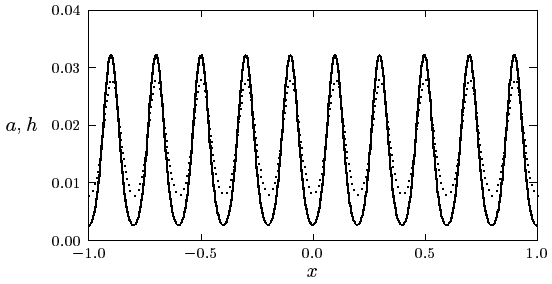

(b) equilibrium state: $D_0 = 3.5$

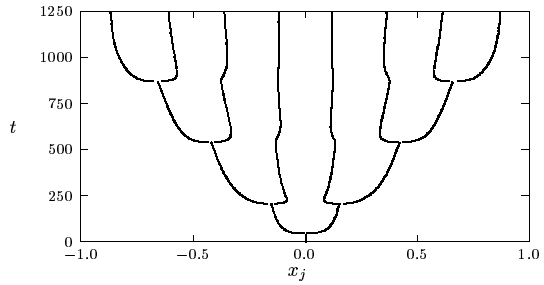

(c) t versus x_j: $D_0 = 3.8$

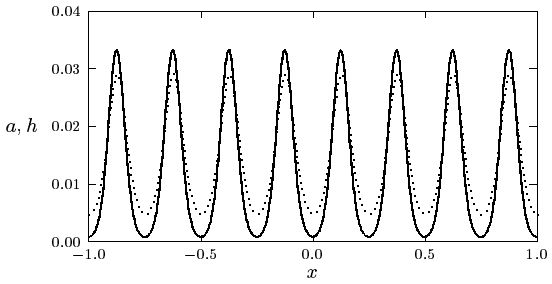

(d) equilibrium state: $D_0 = 3.8$

Figure 10: Experiment 2.2: $(p, q, m, s) = (3, 2, 2, 0)$, $\varepsilon = 0.02$, and $\tau = 0.01$. Top row: plots of t versus x_j, and the final equilibrium state for a (heavy solid curve) and h (dotted curve), for $D_0 = 3.5$. Bottom row: same plot but for $D_0 = 3.8$.

We now perform a simple linearized analysis to try to predict the number of maxima of a in the final equilibrium pattern. We begin by looking for spatially periodic solutions on the whole real line, which bifurcate off of the spatially homogeneous equilibrium solution $a = \varepsilon^{\gamma/\zeta}$ and $h = \varepsilon^{1/\zeta}$. For $\delta \ll 1$, we write

$$a = \varepsilon^{\gamma/\zeta}\left(1 + \delta e^{i\omega x/\varepsilon}\hat{u}\right), \qquad h = \varepsilon^{1/\zeta}\left(1 + \delta e^{i\omega x/\varepsilon}\hat{v}\right), \tag{2.20}$$

for some constants $\hat{u}$ and $\hat{v}$. Without loss of generality we can assume that $\omega > 0$. We substitute (2.20) into the time-independent version of (1.1), and let $D = \varepsilon^2 D_0$. We write the resulting system in the matrix form $A\hat{\mathbf{u}} = 0$. Setting the determinant of A to zero, a simple calculation shows that ω^2 must be a root of the polynomial $f(\omega) = 0$, where

$$f(\omega) = \omega^4 - c\omega^2 + b\,. \tag{2.21a}$$

Here c and b are defined by

$$c \equiv (p-1) - \frac{(1+s)}{D_0}, \qquad b \equiv \frac{(p-1)\zeta}{D_0}, \tag{2.21b}$$

and $\zeta > 0$ is defined in (1.2). Since $b > 0$, there are no roots to $f(\omega) = 0$ when $c < 0$, or equivalently when $D_0 < (1+s)/(p-1)$. Therefore, we assume that $D_0 > (1+s)/(p-1)$. A simple calculation then shows that there are exactly two positive roots $\omega_\pm$ to $f(\omega) = 0$ if and only if $D_0 > D_{h0}$. Therefore, for $D_0 > D_{h0}$, spatially periodic patterns on the infinite line have two possible frequencies. A simple calculation yields

$$D_{h0} \equiv \left(\frac{\sqrt{qm}}{p-1} + \sqrt{\frac{\zeta}{p-1}}\right)^2. \tag{2.22}$$

Numerical values for D_{h0} for different exponent sets were given in the fourth column of Table 1. From this table we observe that $D_{h0} < D_{c0}$, except for the exponent set $(4,2,2,0)$. For $D_0 > D_{h0}$, we then calculate $\omega_\pm$ as

$$0 < \omega_- < \omega_m < \omega_+\,, \qquad \omega_\pm \equiv \left[\frac{c \pm \sqrt{c^2 - 4b}}{2}\right]^{1/2}, \qquad \omega_m \equiv \sqrt{\frac{c}{2}}\,. \tag{2.23}$$

We take the smaller of the two frequencies ω_-, and recall that the length of the domain is two. Then, assuming that D_0 is chosen in the range $D_{h0} < D_0 < D_{c0}$, our prediction is that the number of maxima of a in the final pattern is an integer close to

$$N = \frac{2\omega_-}{2\pi\varepsilon}\,. \tag{2.24}$$

(p,q,m,s)	D_0	ε	N (2.24)	N (observed)
$(2,1,2,0)$	6.0	0.02	9.2	8
$(2,1,2,0)$	6.0	0.03	6.1	6
$(2,1,2,0)$	7.0	0.02	7.6	6
$(2,1,2,0)$	7.0	0.03	5.1	4
$(3,2,2,0)$	3.5	0.02	10.7	10
$(3,2,2,0)$	3.5	0.03	7.0	8
$(3,2,2,0)$	3.8	0.02	9.9	8
$(3,2,2,0)$	3.8	0.03	6.6	6
$(2,2,3,3)$	30.0	0.02	4.65	4
$(3,2,3,1)$	4.0	0.02	11.25	10

Table 2: Comparison of the number of maxima of a in the final equilibrium pattern, from (2.24), versus the observed number, computed numerically from (1.1).

In Table 2 we compare the value of N from (2.24) with the observed number of maxima of a for various pulse-splitting simulations of (1.1). For each case we took $\tau = 0.01$. The initial condition for (1.1) was a one-spike profile. Although the analysis leading to (2.24) was based on a simple linearization around the constant solution the prediction from (2.24) is seen to be relatively close to the actual number of maxima observed. This suggests that the spatially periodic pattern is stable. As a remark, for the exponent set $(4,2,2,0)$ where $D_{h0} > D_{c0}$, our numerical simulation of (1.1) found that the final equilibrium state was a spatially homogeneous solution rather than a periodic pattern.

Our final experiment shows the effect of τ.

Experiment 2.3: Finally, we consider the exponent set $(p,q,m,s) = (2,1,2,0)$ with $D_0 = 7.0$ and $\varepsilon = 0.02$. Recall from Table 1 that there is a Hopf bifurcation at the fold point when $\tau = 1.36$. Hence, for $D_0 = 7.0$ and $\tau = 1.35$, pulse-splitting should be influenced by both the ghost effect of the dimple eigenfunction and the Hopf bifurcation. Starting from a one-spike initial data, in Fig. 11(a) we plot the trajectories of the maxima of a versus t. Upon comparing this figure with Fig. 9(a), where $\tau = 0.01$, we see that pulse-splitting events occur sooner for $\tau = 1.35$. In Fig. 11(b) we show that the amplitude of the spike that is closest to the left endpoint has a significant oscillation near where pulse-splitting occurs. Finally, we perform an identical simulation, but now with $\tau = 1.4$. In Fig. 12 we show that for this value of τ there is no longer any pulse-splitting behavior. Instead the amplitude of the spike at the origin has a time-periodic oscillation.

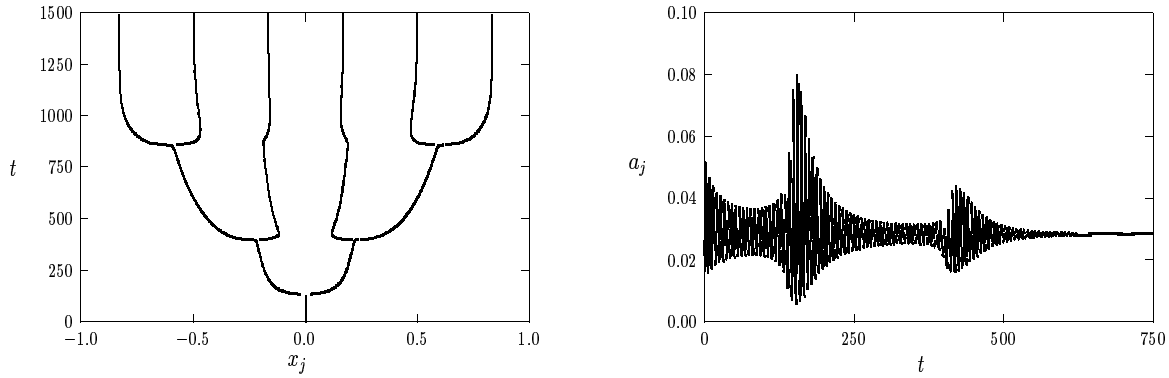

(a) t versus x_j

(b) a and h versus x.

Figure 11: Experiment 2.3: $(p, q, m, s) = (2, 1, 2, 0)$, $D_0 = 7$, $\varepsilon = 0.02$, and $\tau = 1.35$. Left figure: spike trajectories t versus x_j. Right figure: the amplitude $a_m(t) = a(x_1, t)$ for the leftmost spike.

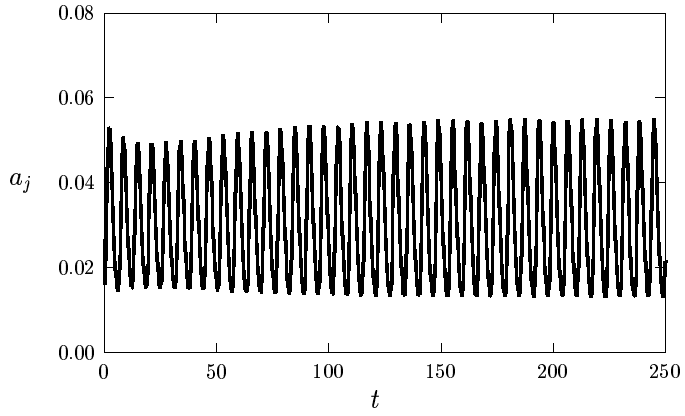

Figure 12: Experiment 2.3: $(p, q, m, s) = (2, 1, 2, 0)$, $D_0 = 7$, $\varepsilon = 0.02$, and $\tau = 1.4$. The amplitude of the spike at the origin versus t. There is no longer any splitting for this larger value of τ.

3 Pulse-Splitting for the Gray-Scott Model: Semi-Strong Limit

In this section we summarize some results of [20] for the analysis of pulse-splitting for the GS model (1.3) in the semi-strong interaction regime. In this regime, and for $A = O(1)$, it was shown in [20] that equilibrium k-spike solutions can be constructed in terms of the solutions $V(y) > 0$ and $U(y) > 0$ to a certain *core problem*, defined in terms of a parameter $B > 0$, by

$$V'' - V + V^2 U = 0\,, \qquad U'' = UV^2\,, \qquad 0 < y < \infty\,, \tag{3.1a}$$

$$V'(0) = U'(0) = 0\,; \quad V \to 0\,, \quad U \sim By\,, \quad \text{as} \quad y \to \infty\,. \tag{3.1b}$$

Therefore, in this particular semi-strong regime, the inner solutions for u and v satisfying (1.3) cannot be decoupled. By matching the inner solution to an appropriate outer solution, A is determined in terms of B by (cf. [20])

$$A \equiv B \coth\left(\theta_0/k\right)\,, \qquad \theta_0 \equiv D^{-1/2}\,. \tag{3.1c}$$

The core problem (3.1a), (3.1b) was first identified in [28] for a one-spike solution to (1.3) on the infinite line. The key relationship (3.1c), relating the infinite-line problem to the finite-line problem, was derived in [20]. In terms of the solution to (3.1), the following equilibrium result was obtained in Proposition 3.1 of [20].

Proposition 3.1: *Let $\varepsilon \to 0$, $A = O(1)$, $\varepsilon A/\sqrt{D} \ll 1$, and suppose that (3.1) has a solution. Then, the v-component for a k-spike equilibrium solution to (1.3) is given by*

$$v \sim \frac{\sqrt{D}}{\varepsilon} \sum_{j=1}^{k} \left(V\left[\varepsilon^{-1}(x - x_j)\right] + O\left(\frac{\varepsilon A}{\sqrt{D}}\right)\right)\,. \tag{3.2}$$

The core problem (3.1) was studied qualitatively and numerically in [20] in terms of B. In [20] it was shown that $0 < \gamma < \frac{3}{2}$, where $\gamma \equiv U(0)V(0)$. Numerical solutions to (3.1) were computed for which V has a single maximum at $y = 0$ as $\gamma \to 3/2$ from below, and a resulting curve $B = B(\gamma)$ was computed. It was shown in [20] (see also [28]), that the curve $B = B(\gamma)$ is double-valued with $B \to 0$ as $\gamma \to 0$ and as $\gamma \to 3/2$, and it has a saddle-node bifurcation point at the maximum value B_c of B given by $B_c = 1.347$, where $\gamma = \gamma_c = 1.02$. We refer to the range $\gamma_c < \gamma < 3/2$ and $0 < \gamma < \gamma_c$ as the *primary* and *secondary* branches of the $B = B(\gamma)$ bifurcation diagram. From (3.1a) it is clear that V has a double-bump structure on the range $0 < \gamma < 1$ of the secondary branch. Since $B \equiv A \tanh\left(\theta_0/k\right)$ from (3.1b), these results of [20] show that equilibrium k-spike solutions exist only when A is small enough. In particular, we have (cf. Proposition 3.2 of [20]):

Proposition 3.2: *Let $\varepsilon \ll 1$, $A = O(1)$, and $\varepsilon A/\sqrt{D} \ll 1$. Then, there will be no k-spike equilibrium solution to (1.3) that merges onto the solution in the regime $A \ll 1$ when*

$$A > A_{pk} \equiv 1.347 \coth\left(\frac{1}{k\sqrt{D}}\right) . \tag{3.3}$$

In terms of the solution to the core problem, we define a norm by

$$|v|_2 \equiv \left(\int_{-1}^{1} v^2\, dx\right)^{1/2} \sim \sqrt{\frac{kD}{\varepsilon}} \left(\int_{-\infty}^{\infty} V^2\, dy\right)^{1/2} . \tag{3.4}$$

In Fig. 2(a) of §1 we plotted this norm for $D = 0.1$, $A = 2.4$, $\varepsilon = 0.01$, and $k = 1, 2, 3, 4$. On this figure, the portions of the branches where v has a two-bump profile in the core is shown by the dotted lines. From this figure, and from (3.3), it is clear that the *lining-up property* of [11] holds now only in an approximate sense, and that the *multi-bump transition condition* is satisfied. It was verified numerically in [20] that the *dimple property* of [11] holds at the fold point. In addition, a lengthy analytical calculation in [20] shows that the secondary branch is unconditionally unstable, while the primary branch is stable only for $\tau \ll O(\varepsilon^{-1})$. Thus, the pulse-splitting criteria of [11] are satisfied when $\tau \ll O(\varepsilon^{-1})$. The following conjecture was then made in [20]:

Conjecture 3.3: *Let $\varepsilon \ll 1$, $A = O(1)$, $\tau \ll O(\varepsilon^{-1})$, and $\varepsilon A/\sqrt{D} \ll 1$. Suppose that we have even one-spike initial data centered at the origin. Then, the final equilibrium state is stable, and it has 2^m spikes where, for some integer $m \geq 0$, A is related to A_{pk} by*

$$A_{p2^{m-1}} < A < A_{p2^m} . \tag{3.5}$$

We now perform a few numerical experiments using the NAG routine D03PCF (cf. [29]) to illustrate both (3.5) and the pulse-splitting behavior. In the examples below, we fix ε, τ, and A, and consider the effect of taking smaller values of D. The initial condition for v is taken to be an even function localized near $x = 0$.

Experiment 3.1: Let $\varepsilon = 0.01$, $\tau = 2.0$, and $A = 2.4$. For the following two values of D we calculate A_{pk} and $\varepsilon A/\sqrt{D}$:

$$D = 0.75\,; \qquad A_{p1} = 1.64\,, \quad A_{p2} = 2.59\,, \quad A_{p4} = 4.79\,, \quad \frac{\varepsilon A}{\sqrt{D}} = 0.028\,, \tag{3.6a}$$

$$D = 0.25\,; \qquad A_{p1} = 1.39\,, \quad A_{p2} = 1.77\,, \quad A_{p4} = 2.91\,, \quad \frac{\varepsilon A}{\sqrt{D}} = 0.048\,. \tag{3.6b}$$

Therefore, from (3.5), we predict a two-spike final equilibrium state when $D = 0.75$, and a four-spike equilibrium state when $D = 0.25$. This is shown in Fig. 13(a). In Fig. 13(b) we plot the final

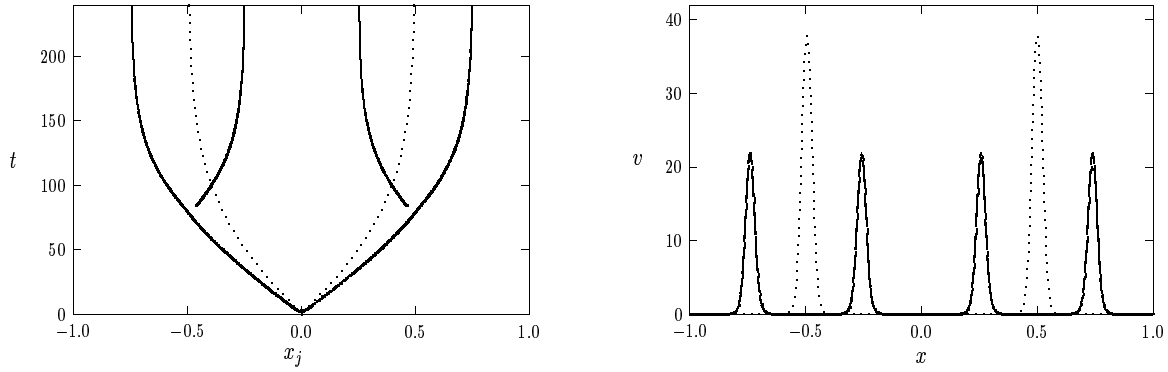

(a) t versus x_j (b) v versus x

Figure 13: Experiment 3.1: Simultaneous splitting for the v component in the GS model for $\varepsilon = 0.01$, $\tau = 2.0$, and $A = 2.4$. Left figure: t versus x_j. Right figure: the final equilibrium state. The dotted curves are for $D = 0.75$, while the heavy solid curve is for $D = 0.25$.

equilibrium state for v for each of these two values of D. For this semi-strong spike interaction regime, the pulse-splitting behavior is a simultaneous splitting process and the final equilibrium state is a spike-type pattern.

Experiment 3.2: Next, we let $\varepsilon = 0.01$, $\tau = 2.0$, and $A = 2.4$, and we choose the smaller value $D = 0.1$. This is the example shown in Fig. 2(b) of §1. The values for A_{pk} and $\varepsilon A/\sqrt{D}$ are

$$D = 0.1\,; \qquad A_{p1} = 1.35\,, \quad A_{p2} = 1.47\,, \quad A_{p4} = 2.04\,, \quad A_{p8} = 3.58\,, \quad \frac{\varepsilon A}{\sqrt{D}} = 0.076\,. \tag{3.7}$$

Since $A_{p4} < A < A_{p8}$, the criterion (3.5) correctly predicts an eight-spike final equilibrium state. In Fig. 14 we plot the v component of the solution at different times showing a roughly simultaneous splitting process.

Experiment 3.3: Next, we consider the effect of decreasing D further. We take the same parameter set $\varepsilon = 0.01$, $\tau = 2.0$, $A = 2.4$, but now we choose $D = 0.01$. We calculate

$$D = 0.01\,; \qquad A_{p2} = 1.347\,, \quad A_{p4} = 1.365\,, \quad A_{p8} = 1.588\,, \quad A_{p16} = 2.43\,, \quad \frac{\varepsilon A}{\sqrt{D}} = 0.24\,. \tag{3.8}$$

In this case, the criterion (3.5) erroneously predicts a 16-spike final equilibrium state. However, for this example we have $\varepsilon A/\sqrt{D} = O(1)$, and so the analysis leading to the criterion (3.1), which

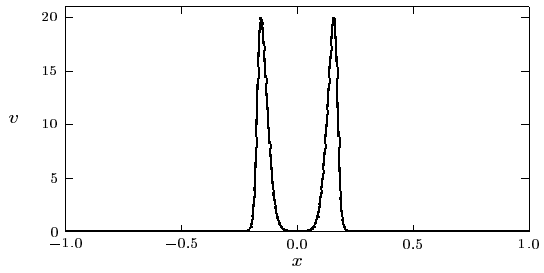

(a) $t = 20$

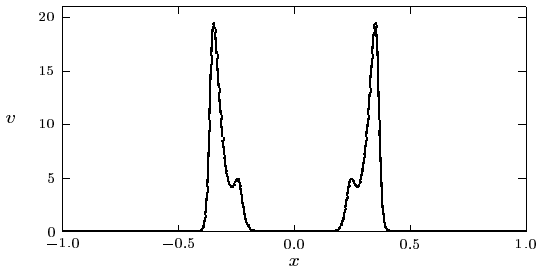

(b) $t = 45$

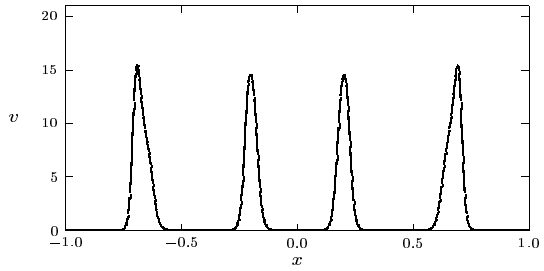

(c) $t = 100$

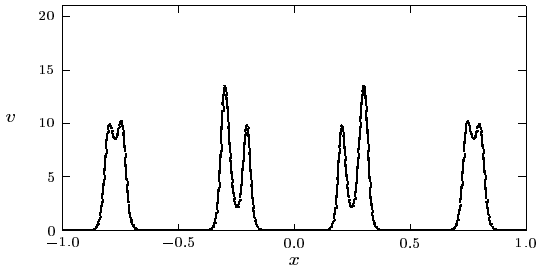

(d) $t = 150$

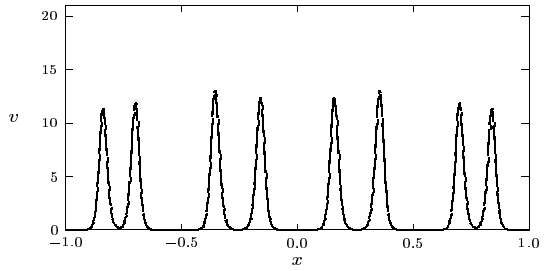

(e) $t = 175$

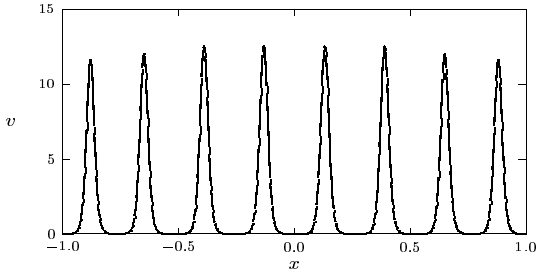

(f) $t = 225$

Figure 14: Experiment 3.2: Simultaneous pulse-splitting for the v component in the GS model for the parameter set $\varepsilon = 0.01$, $\tau = 2.0$, $A = 2.4$, and $D = 0.1$. The final plot when $t = 225$ is very close to the equilibrium state.

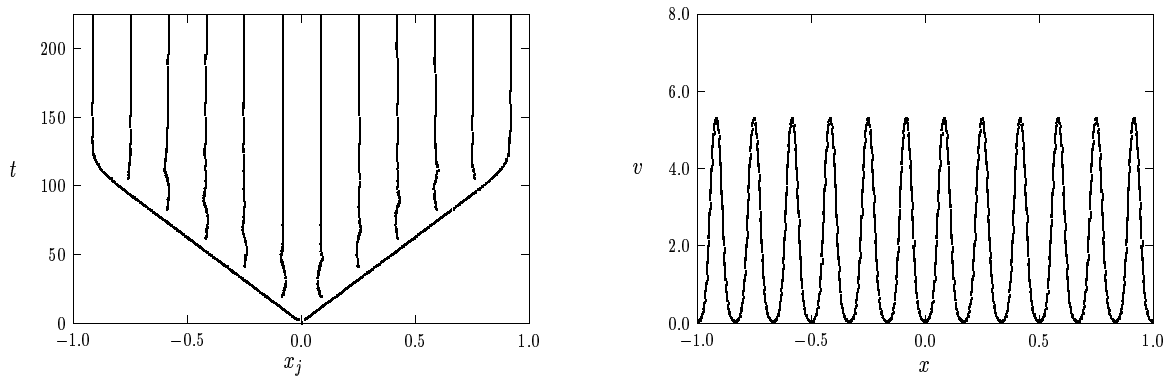

(a) t versus x_j

(b) v versus x

Figure 15: Experiment 3.3: Edge-splitting for the GS model for the parameter set $\varepsilon = 0.01$, $\tau = 2.0$, $A = 2.4$, and $D = 0.01$. Left figure: t versus x_j. Right figure: plot of v close to the equilibrium state.

assumes semi-strong spike interactions, is not valid. In Fig. 15 we plot t versus x_j and the final equilibrium state. The final equilibrium state more closely resembles a periodic solution than a spike pattern. In Fig. 16 we plot the v component of the solution at different times showing an edge-splitting pulse-replication process. The figures are very similar to those computed in §2 for the GM model in the weak interaction regime. For the GS model, edge-splitting was observed in all of the numerical computations of [31] in the weak interaction regime.

For the GS model, this series of experiments clearly shows that edge-splitting occurs in the weak interaction regime, while a simultaneous splitting process occurs in the semi-strong interaction regime. Therefore, there must be a range of values of D, with $D = O(\varepsilon^{2-\nu})$ for $0 < \nu < 2$, where both types of splitting behaviors is observed. This is shown in our final example.

Experiment 3.4: We take the parameter set $\varepsilon = 0.01$, $\tau = 2.0$, $A = 2.4$, but now with $D = 0.035$. In Fig. 17 we plot t versus x_j and the final equilibrium state. Notice here that the splitting process is neither pure edge-splitting or simultaneous splitting, but rather has elements of both processes. The final equilibrium state has ten spikes. For this parameter set, we calculate $A_{p8} = 2.31$ and $A_{p16} = 4.19$. Since $A_{p8} < A < A_{p16}$, (3.5) erroneously predicts a 16-spike final equilibrium state. However, since $\frac{\varepsilon A}{\sqrt{D}} = 0.13$ is not particularly small, the validity of (3.5) is indeed questionable.

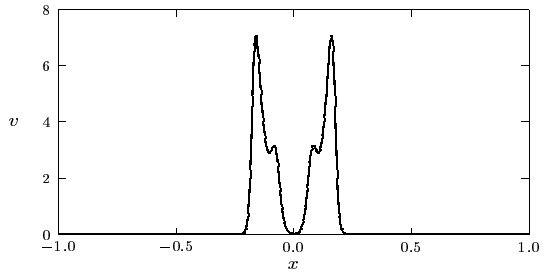

(a) $t = 20$

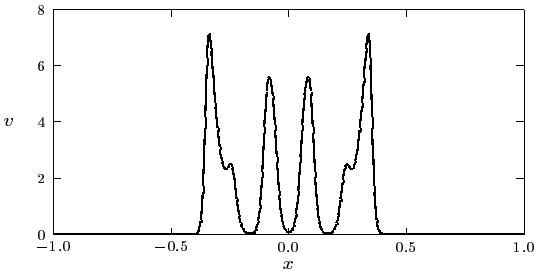

(b) $t = 42$

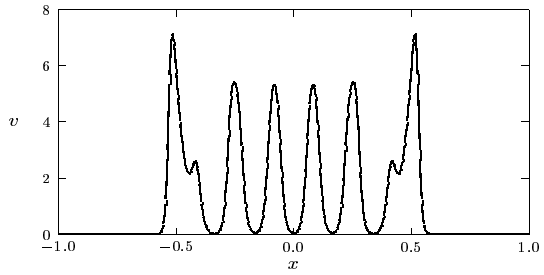

(c) $t = 64$

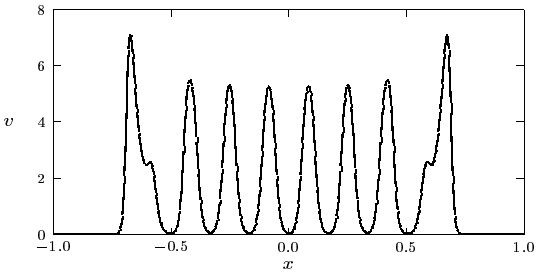

(d) $t = 84$

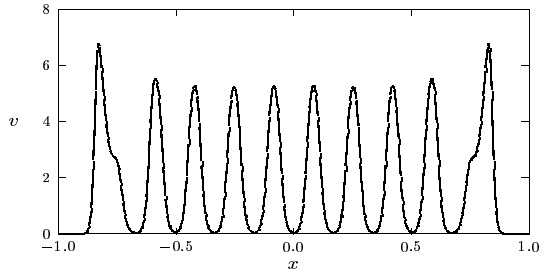

(e) $t = 104$

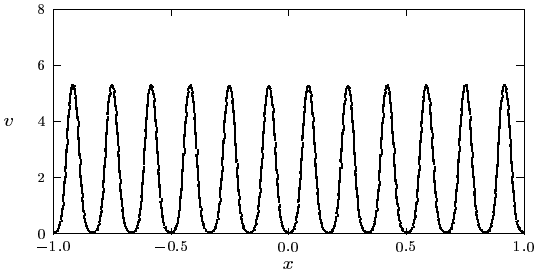

(f) $t = 220$

Figure 16: Experiment 3.3: Edge-splitting for the v component in the GS model for the parameter set $\varepsilon = 0.01$, $\tau = 2.0$, $A = 2.4$, and $D = 0.01$. The final plot when $t = 220$ is very close to the equilibrium state.

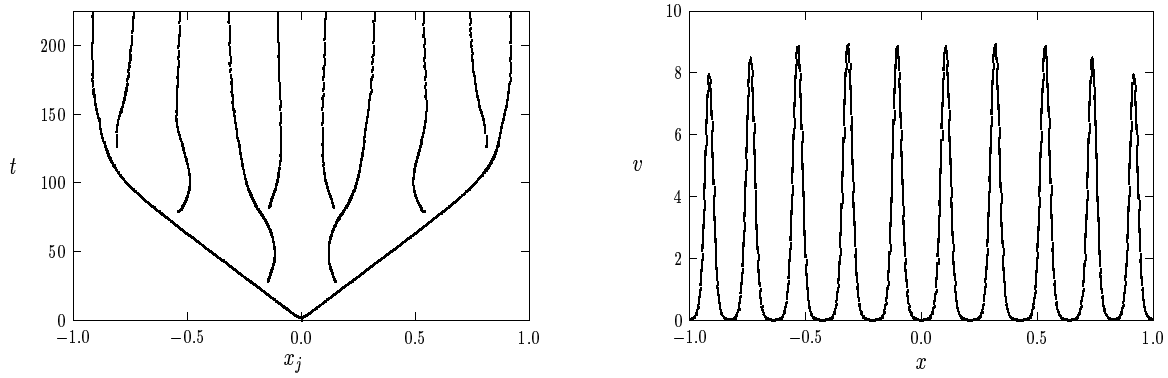

(a) t versus x_j (b) v versus x

Figure 17: Experiment 3.4: Both types of splitting for the GS model for the parameter set $\varepsilon = 0.01$, $\tau = 2.0$, $A = 2.4$, and $D = 0.035$. Left figure: t versus x_j. Right figure: plot of v close to the equilibrium state.

We now show numerically that the bifurcation diagram for a one-spike solution to (1.3) has a topological change as D decreases, thereby invalidating (3.5). We compute a one-spike equilibrium solution to

$$\varepsilon^2 v_{xx} - v + Av^2 u = 0\,, \quad Du_{xx} - u + 1 - v^2 u = 0\,, \quad -1 < x < 1\,; \qquad u_x(\pm 1) = v_x(\pm 1) = 0\,. \tag{3.9}$$

For $\varepsilon A/\sqrt{D} \ll 1$ there is a fold point at A_{p1} given in (3.3) (cf. [20]). Moreover, for $D = O(1)$, there is also another fold point at $A_{e1} = O(\varepsilon^{1/2})$ (cf. [19]), where

$$A_{e1} = \sqrt{\frac{12\varepsilon}{\sqrt{D}} \coth\left(\frac{1}{\sqrt{D}}\right)}\,. \tag{3.10}$$

When $D = O(1)$, the fold point at A_{e1} is not related to pulse-splitting behavior (cf. [19]). However, the asymptotic behavior of A_{e1} for $D \ll 1$, as obtained from (3.10), suggests that A_{e1} and A_{p1} may coalesce as $D \to 0$, leading to a topological change in the bifurcation diagram for a one-spike solution of (3.9). For $\varepsilon = 0.01$, in Fig. 18 we plot the numerically computed fold points as a function of p when $D = \varepsilon^p$. In this figure it is clear that the asymptotic approximations (3.3) and (3.10) for A_{p1} and A_{e1}, respectively, fail as $p \to 2$. This behavior provides the transition between the semi-strong spike interaction regime and the weak interaction regime of [31], [32], and [40].

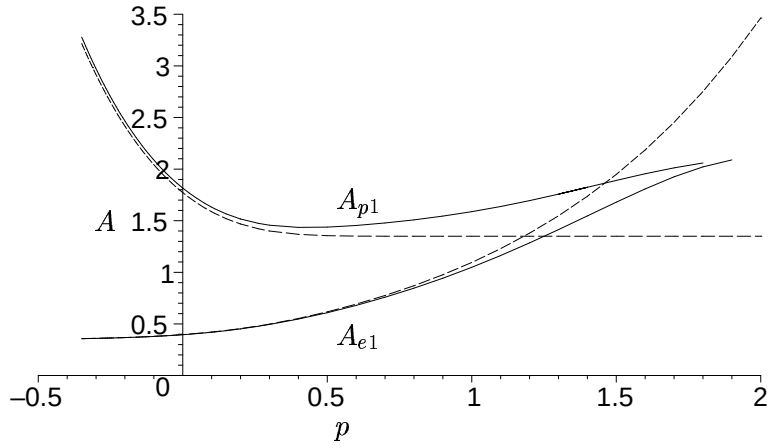

Figure 18: Plots of the fold points A_{p1} and A_{e1} versus p, where $D = \varepsilon^p$ and $\varepsilon = 0.01$. The two fold points merge as $p \to 2$. The asymptotic results, valid for $D = O(1)$, are the dotted curves, and the full numerical results are the solid curves.

It is beyond our scope here to describe the dynamical mechanisms of pulse-splitting in the semi-strong regime. Much work on this topic still needs to be done. The earliest study of the dynamics of pulse-splitting, based on formal asymptotics, was given in [36] and [37]. A mostly qualitative discussion is given in [5].

4 Pulse-Splitting Criteria: A Semi-Strong RD Model I

In this section we consider the following model reaction-diffusion system;

$$a_t = \varepsilon^2 a_{xx} - a + a^p - ah\,, \qquad -1 < x < 1\,, \quad t > 0\,, \tag{4.1a}$$

$$\tau h_t = Dh_{xx} - h + \varepsilon^{-1}\mu\sqrt{D}\frac{a^2}{(1+h)^s}\,, \qquad -1 < x < 1\,, \quad t > 0\,, \tag{4.1b}$$

$$a_x(\pm 1, t) = h_x(\pm 1, t) = 0\,; \qquad a(x,0) = a_0(x)\,, \qquad h(x,0) = h_0(x)\,. \tag{4.1c}$$

In (4.1), $0 < \varepsilon \ll 1$, $D > 0$, $\mu > 0$, and $\tau \geq 0$, are constants, and $D = O(1)$ as $\varepsilon \to 0$. The exponents (p, s) are assumed to satisfy $s \geq -3/2$ and $1 \leq p - 1 < 4/(3 + 2s)$. The reason for this range of exponents is explained below in (4.16). Since $\varepsilon \ll 1$ and $D = O(1)$, this system is of the form (1.5), which admits semi-strong spike interactions.

For this system, we construct k-spike equilibria and we analyze their stability properties. The analysis shows that all of the pulse-splitting criteria of [11] hold in the same approximate sense

as for the GS model in §3. However, the *multi-bump transition condition of §1* is not satisfied. Numerical experiments do not reveal pulse-splitting behavior for this model.

4.1 The Equilibrium Problem

For $\varepsilon \to 0$, we use the method of matched asymptotic expansions to construct a symmetric k-spike equilibrium solution to (4.1) where the spikes have equal height. From symmetry considerations, the spike locations x_j, for $j = 1, \ldots, k$, satisfy

$$x_j = -1 + \frac{(2j-1)}{k}\,, \qquad j = 1, \ldots, k\,. \tag{4.2}$$

In addition, $a'(x_j) = 0$ and $h(x_j) = H$, for $j = 1, \ldots, k$, where H is independent of j.

In the inner region near the j^{th} spike we introduce new variables by

$$y_j \equiv \varepsilon^{-1}(x - x_j)\,, \qquad \tilde{h}(y_j) \equiv h(x_j + \varepsilon y)\,, \qquad \tilde{a}(y_j) \equiv a(x_j + \varepsilon y)\,, \tag{4.3a}$$

and we expand

$$\tilde{h}(y_j) = \tilde{h}_0(y_j) + \varepsilon \tilde{h}_1(y_j) + \ldots\,, \qquad \tilde{a}(y_j) = \tilde{a}_0(y_j) + O(\varepsilon)\,. \tag{4.3b}$$

Substituting (4.3) into the equilibrium problem for (4.1), we collect powers of ε to get $\tilde{h}_0'' = 0$. Therefore, $\tilde{h}_0 = H$, where H is to be found. In addition, we get on $-\infty < y_j < \infty$ that

$$\tilde{a}_0'' - \tilde{a}_0 + \tilde{a}_0^p - \tilde{a}_0 H = 0\,; \qquad D\tilde{h}_1'' = -\mu\sqrt{D}\,\frac{\tilde{a}_0^2}{(1+H)^s}\,. \tag{4.4}$$

The solution for $\tilde{a}_0$, with $\tilde{a}_0'(0) = 0$, is simply

$$\tilde{a}_0 = (1+H)^{\gamma}\, w\left[\sqrt{1+H}\, y_j\right]\,, \qquad \gamma \equiv 1/(p-1)\,. \tag{4.5}$$

Here $w(\xi)$ is the unique positive solution to

$$w'' - w + w^p = 0\,, \quad -\infty < \xi < \infty\,; \qquad w \to 0 \quad \text{as} \quad |\xi| \to \infty\,; \qquad w'(0) = 0\,, \quad w(0) > 0\,. \tag{4.6}$$

The explicit solution to (4.6) is given in (2.2b). We then use (4.5) and (2.2b) to calculate

$$\mu\sqrt{D}\int_{-\infty}^{\infty} \frac{\tilde{a}_0^2}{(1+h_0)^s}\, dy_j \sim \mu\sqrt{D}\,(1+H)^{2\gamma - s - 1/2}\; I_p\,. \tag{4.7a}$$

Here, I_p is defined in terms of the Gamma function $\Gamma(z)$ by

$$I_p \equiv \int_{-\infty}^{\infty} [w(\xi)]^2\, d\xi = \left(\frac{p+1}{p-1}\right)\left(\frac{p+1}{2}\right)^{\frac{2}{p-1}-1} \frac{\Gamma\left(\frac{2}{p-1}\right)\Gamma\left(\frac{1}{2}\right)}{\Gamma\left(\frac{2}{p-1}+\frac{1}{2}\right)}\,. \tag{4.7b}$$

By integrating the equation for $\tilde{h}_1$ in (4.4), and by using (4.7a), we obtain

$$\lim_{y_j \to +\infty} \tilde{h}_1' - \lim_{y_j \to -\infty} \tilde{h}_1' = -\frac{\mu}{\sqrt{D}} (1+H)^{2\gamma - s - 1/2} I_p \,. \tag{4.8}$$

This equation yields a jump condition for the outer solution for h.

In the outer region, defined away from $O(\varepsilon)$ regions near each x_j, a is exponentially small, and h is expanded as $h(x) = h_0(x) + o(\varepsilon)$, where h_0 satisfies $Dh_0'' - h_0 = 0$ on $-1 < x < 1$. Upon matching to the inner solution constructed above, we obtain that h_0 is continuous across each x_j, but that the jump in h_0' at $x = x_j$ is given by the right-hand side of (4.8). Therefore, in terms of the delta function $\delta(x)$, h_0 satisfies

$$Dh_0'' - h_0 = -\mu\sqrt{D}\,(1+H)^{2\gamma - s - 1/2}\; I_p \sum_{j=1}^{k} \delta(x - x_j)\,, \quad -1 < x < 1\,; \qquad h_0'(\pm 1) = 0\,. \tag{4.9}$$

The solution to (4.9) can be written as

$$h_0(x) = \mu\sqrt{D}\,(1+H)^{2\gamma - s - 1/2}\; I_p \sum_{j=1}^{k} G_0(x; x_j)\,, \tag{4.10}$$

where $G_0(x; x_j)$ is the Green's function satisfying

$$DG_{0xx} - G_0 = -\delta(x - x_j)\,, \quad -1 < x < 1\,; \quad G_{0x}(\pm 1; x_j) = 0\,. \tag{4.11}$$

The matching condition requires that $h_0(x_i) = H$ for $i = 1, \ldots, k$. Therefore, using (4.10), and the simple identity (cf. [16]),

$$\sum_{j=1}^{k} G_0(x_i; x_j) \equiv a_g = \left[2\sqrt{D} \tanh\left(\theta_0/k\right) \right]^{-1}\,, \quad i = 1, \ldots, k\,, \tag{4.12}$$

we find that H satisfies the nonlinear algebraic equation

$$H = (1+H)^{2\gamma - s - 1/2} \left(\frac{\mu I_p}{2\tanh\left(\theta_0/k\right)} \right)\,. \tag{4.13}$$

To study (4.13), it is convenient to define $c > 0$ and $\beta > 0$ by

$$c \equiv \sqrt{H+1}\,, \qquad \beta \equiv \frac{\mu I_p}{2\tanh\left(\theta_0/k\right)}\,, \tag{4.14}$$

where I_p is defined in (4.7b). Then, from (4.13), $c > 0$ is a root of $f(c) = 0$, where

$$f(c) \equiv \beta c^{4\gamma - 2s - 1} - c^2 + 1 \,. \tag{4.15}$$

There are two k-spike equilibria to (4.1) when (4.15) has two positive roots. Since $f(0) = 1$, this is only possible when $f(c) \to +\infty$ as $c \to \infty$. Hence, we will assume that p and s are such that $4\gamma - 2s - 1 > 2$. With $\gamma = 1/(p-1)$, and $p \geq 2$, this implies that

$$2 \leq p < 1 + \frac{4}{3 + 2s} \,. \tag{4.16}$$

Next, we set $f'(c_m) = 0$, to get

$$c_m = \left[\frac{2}{\beta(4\gamma - 2s - 1)} \right]^{1/(4\gamma - 2s - 3)} \,. \tag{4.17}$$

If $f(c_m) < 0$, then there are two positive roots c_+ and c_- to $f(c) = 0$. This occurs when

$$0 < \beta < \beta_c \equiv \frac{2}{4\gamma - 2s - 1} \left(\frac{4\gamma - 2s - 3}{4\gamma - 2s - 1} \right)^{2\gamma - s - 3/2} \,. \tag{4.18}$$

Alternatively, when $\beta > \beta_c$, then $f(c_m) > 0$ and there are no positive roots to $f(c) = 0$. When this condition holds there are no k-spike equilibrium solutions to (4.1). Notice also that $f(1) = \beta > 0$ and $f(c_*) = 1$, where $\beta c_*^{4\gamma - 2s - 3} = 1$. The critical value β_c yields a critical value for μ in terms of D from (4.14). We summarize the properties of the roots of $f(c) = 0$ as follows:

Lemma 4.1: *Let p and s satisfy (4.16). Define the critical value μ_k by*

$$\mu_k \equiv \frac{4 \tanh(\theta_0/k)}{(4\gamma - 2s - 1) I_p} \left(\frac{4\gamma - 2s - 3}{4\gamma - 2s - 1} \right)^{2\gamma - s - 3/2} \,, \qquad \theta_0 = D^{-1/2} \,. \tag{4.19}$$

Suppose that $0 < \mu < \mu_k$. Then, there are positive roots $c_\pm$ to $f(c) = 0$, satisfying

$$1 < c_- < c_m < c_+ < c_* \,. \tag{4.20}$$

When $\mu > \mu_k$, there are no positive roots to $f(c) = 0$.

When $\mu < \mu_k$, then from (4.14) we have two values for H given by $H_\pm = c_\pm^2 - 1$. The resulting two k-spike equilibrium solutions are obtained from (4.5) and (4.10). This leads to the following equilibrium result for (4.1):

Proposition 4.2: *Let $0 < \varepsilon \ll 1$, with p and s satisfying (4.16). Then, when $\mu > \mu_k$ there are no symmetric k-spike equilibria to (4.1). For $0 < \varepsilon \ll 1$ and $0 < \mu < \mu_k$, there are exactly two symmetric k-spike equilibria to (4.1) labeled by $a_{e\pm}$ and $h_{e\pm}$. They are given asymptotically by*

$$a_{e\pm}(x) \sim (1+H_\pm)^\gamma \sum_{j=1}^{k} w\left[\sqrt{1+H_\pm}\,\varepsilon^{-1}(x-x_j)\right], \qquad \gamma = 1/(p-1), \tag{4.21a}$$

$$h_{e\pm}(x) \sim \frac{H_\pm}{a_g}\sum_{j=1}^{k} G_0(x;x_j), \quad |x-x_i| \gg O(\varepsilon), \quad x_i = -1 + \frac{(2i-1)}{k}. \tag{4.21b}$$

Here $w(\xi)$, G_0, and a_g, satisfy (4.6), (4.11), and (4.12), respectively. Moreover, $H_\pm = c_\pm^2 - 1$, where $c_\pm$ are the two positive roots of $f(c) = 0$ as given in Lemma 4.1.

Therefore, when p and s satisfy (4.16), there is a saddle-node bifurcation structure for k-spike equilibria of (4.1) in terms of the parameter μ. Using (4.7b), (4.14), and (4.19), we calculate

$$\beta_c = \frac{2\sqrt{3}}{9}, \quad \mu_k = \frac{2\sqrt{3}}{27}\tanh\left(\frac{\theta_0}{k}\right), \quad \text{for} \quad (p,s) = (2,0), \tag{4.22a}$$

$$\beta_c = \frac{2\sqrt{3}}{9}, \quad \mu_k = \frac{\sqrt{3}}{9}\tanh\left(\frac{\theta_0}{k}\right), \quad \text{for} \quad (p,s) = (3,-1). \tag{4.22b}$$

Here we have used the value $I_3 = 4$, as obtained from (4.7b). Numerical values for μ_k^{-1} are given in Table 3.

To illustrate our results graphically, it is convenient to use (2.2b) and define a norm of $a_{e\pm}$ by

$$|a|_2 \equiv \left(\sum_{j=1}^{k}\left[a_{e\pm}(x_j)\right]^2\right)^{1/2} \sim (1+H_\pm)^\gamma\, w(0)\sqrt{k} = (1+H_\pm)^\gamma \left(\frac{p+1}{2}\right)^{1/(p-1)}\sqrt{k}. \tag{4.23}$$

In Fig. 19(a) we plot $|a|_2$ versus μ^{-1} when $D = 0.25$, $p = 2$, and $s = 0$, for a k-spike solution with $k = 1, 2, 3$. The top portion of each of these solution branches corresponds to the *large* solution a_{e+}, while the bottom portion corresponds to the *small* solution a_{e-}. The values of μ^{-1} at the fold points are given in the first row of Table 3. The segments of these branches that are unstable on an $O(1)$ time-scale are labeled by the dotted lines. These stability results are obtained below in the next subsection.

When $D \ll 1$, so that $\theta_0 \gg 1$, we observe that $\tanh(\theta_0/k) \approx 1$. Therefore, μ_k is approximately independent of k for a finite number of k, and so the fold points for a finite number of branches of equilibria occur at approximately the same value of μ. This is an approximate *lining-up property*

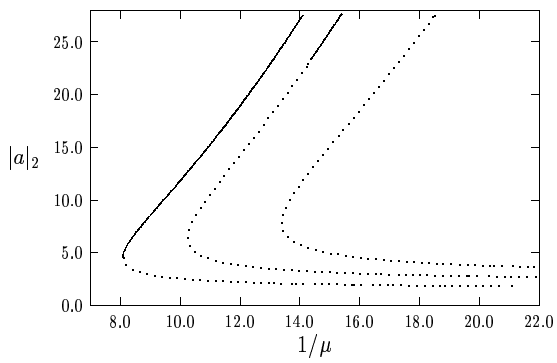

(a) $|a|_2$ for $k = 1, 2, 3$

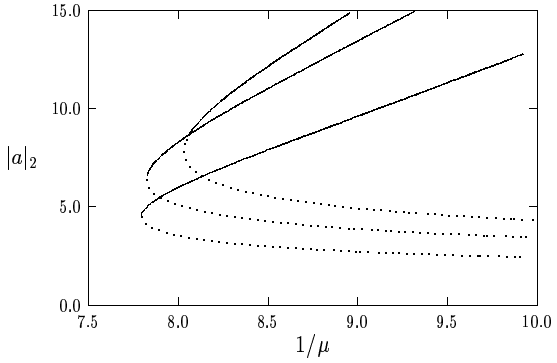

(b) $|a|_2$ for $k = 1, 2, 3$

Figure 19: Left figure: the norm $|a|_2$, defined in (4.23), versus μ^{-1} for $k = 1, 2, 3$, when $D = 0.25$, $p = 2$, and $s = 0$. Right figure: identical plot, but for $D = 0.025$. In both figures, the portions of the branches that are unstable on an $O(1)$ time-scale are indicated by the dotted lines.

for k-spike equilibria. In Fig. 19(b) we plot $|a|_2$ versus μ^{-1} for $k = 1, 2, 3$ when $D = 0.025$, $p = 2$, and $s = 0$. For this value of D, the fold point values are given in the second row of Table 3. In Fig. 19(b), the portions of these branches that are unstable when $\tau = 0$ are indicated by the dotted lines.

In Fig. 20(a) and Fig. 20(b) we plot $a_{e\pm}$ and $h_{e\pm}$, obtained from (4.21), for a one-spike solution with $D = 0.25$, $p = 2$, $s = 0$, $\mu^{-1} = 9.1$, and $\varepsilon = 0.05$. For these parameter values, we use Newton's method to find the zeroes of (4.15). This yields, $c_+ = 2.424$ and $c_- = 1.374$. It is clear from (4.21) and from this figure that the *multi-bump transition condition* of §1 does not hold.

(p, s)	D	$k = 1$	$k = 2$	$k = 3$
$(2, 0)$	0.25	8.09	10.2	13.4
$(2, 0)$	0.025	7.79	7.82	8.03
$(3, -1)$	0.25	5.39	6.82	8.92
$(3, -1)$	0.025	5.20	5.21	5.35

Table 3: Numerical values for μ_k^{-1}, computed from (4.19), for two values of D and exponents (p, s).

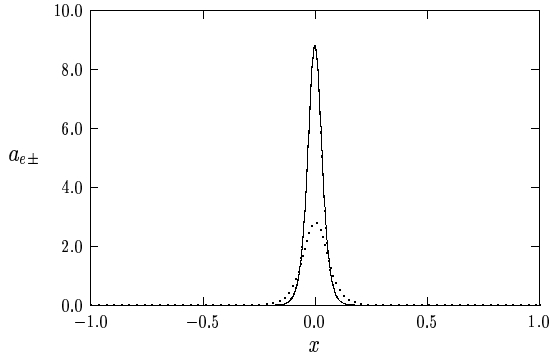

(a) $a_{e\pm}$ for $k = 1$

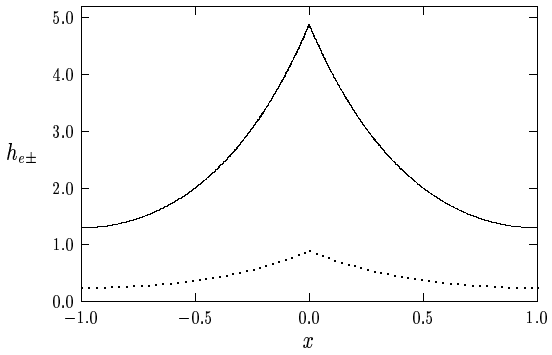

(b) $h_{e\pm}$ for $k = 1$

Figure 20: Plots of $a_{e\pm}$ and $h_{e\pm}$ versus x for a one-spike solution with $D = 0.25$, $\mu^{-1} = 9.1$, $p = 2$, $s = 0$, and $\varepsilon = 0.05$. The solid curves correspond to the large solution a_{e+} and h_{e+}, while the dotted curves correspond to the small solution a_{e-} and h_{e-}.

4.2 The Stability of k-Spike Equilibria

Next, we analyze the stability of the equilibria constructed above. We substitute $a = a_{e\pm} + e^{\lambda t}\phi$ and $h = h_{e\pm} + e^{\lambda t}\eta$ into (4.1), where $\phi \ll 1$ and $\eta \ll 1$. This leads to the eigenvalue problem

$$\varepsilon^2\phi_{xx} - \phi + pa_{e\pm}^{p-1}\phi - a_{e\pm}\eta - h_{e\pm}\phi = \lambda\phi\,, \quad -1 < x < 1\,, \tag{4.24a}$$

$$D\eta_{xx} - (1+\tau\lambda)\eta = -2\varepsilon^{-1}\mu\sqrt{D}\frac{a_{e\pm}\phi}{(1+h_{e\pm})^s} + \varepsilon^{-1}s\mu\sqrt{D}\frac{a_{e\pm}^2\eta}{(1+h_{e\pm})^{s+1}}\,, \quad -1 < x < 1\,, \tag{4.24b}$$

$$\phi_x(\pm 1) = \eta_x(\pm 1) = 0\,. \tag{4.24c}$$

The spectrum of (4.24) contains two classes of eigenvalues. There are the large eigenvalues that are $O(1)$ as $\varepsilon \to 0$, and the small eigenvalues that are $O(\varepsilon^2)$ as $\varepsilon \to 0$. Since we are only interested in determining instabilities that occur on a fast $O(1)$ time-scale, we will only analyze the spectrum of (4.24) associated with the large eigenvalues. We begin by deriving a nonlocal eigenvalue problem that governs the stability of the equilibrium solution with respect to these eigenvalues.

To do so, we look for a localized eigenfunction for ϕ in the form

$$\phi(x) \sim \sum_{j=1}^{k} b_j \Phi\left[\sqrt{1+H_\pm}\,\varepsilon^{-1}(x-x_j)\right], \tag{4.25}$$

for some coefficients b_j, $j=1,\ldots,k$. Since ϕ is localized near each x_j when $\varepsilon \ll 1$, the two terms on the right-hand side of (4.24b) are multiples of a Dirac mass near each x_j. We use (4.21a) for $a_{e\pm}$ to calculate these multiples. In this way, we obtain that η satisfies

$$D\eta_{xx} - (1+\tau\lambda)\,\eta = 0\,, \qquad x_{j-1} < x < x_j\,, \quad j=1,\ldots,k+1\,, \tag{4.26a}$$

$$[\eta]_j = 0\,, \quad [D\eta_x]_j = -\omega_j + g\eta(x_j)\,, \quad j=1,\ldots,k\,; \qquad \eta_x(\pm 1) = 0\,. \tag{4.26b}$$

In (4.26), we have defined $x_0 \equiv -1$, $x_{k+1} \equiv 1$, $[v]_j \equiv v(x_{j+}) - v(x_{j-})$, together with

$$\omega_j \equiv 2\mu\sqrt{D}\,b_j\,c_\pm^{2\gamma-2s-1}\int_{-\infty}^{\infty} w(\xi)\Phi(\xi)\,d\xi\,, \quad j=1,\ldots,k\,; \qquad g \equiv s\mu\sqrt{D}\,c_\pm^{4\gamma-2s-3}I_p\,. \tag{4.27}$$

Here $c_\pm$ are the positive roots of $f(c)=0$ as given in Lemma 4.1.

To determine the eigenvalue problem for λ, we must calculate $\eta(x_j)$ from (4.26). To do so, we solve (4.26a) on each subinterval and use the boundary and jump conditions in (4.26b). This calculation results in the matrix problem

$$\mathcal{B}_s\boldsymbol{\eta} = \frac{\boldsymbol{\omega}}{[(1+\tau\lambda)D]^{1/2}}\,, \quad \mathcal{B}_s \equiv \mathcal{B} + \frac{g}{[(1+\tau\lambda)D]^{1/2}}I\,, \quad \boldsymbol{\eta} \equiv \begin{pmatrix} \eta(x_1) \\ \vdots \\ \eta(x_k) \end{pmatrix}\,, \quad \boldsymbol{\omega} \equiv \begin{pmatrix} \omega_1 \\ \vdots \\ \omega_k \end{pmatrix}\,, \tag{4.28}$$

where I is the identity matrix. The matrix $\mathcal{B}$ in (4.28) is tridiagonal and has the explicit form

$$\mathcal{B} \equiv \begin{pmatrix} d_\lambda & f_\lambda & 0 & \cdots & 0 & 0 & 0 \\ f_\lambda & e_\lambda & f_\lambda & \cdots & 0 & 0 & 0 \\ 0 & f_\lambda & e_\lambda & \ddots & 0 & 0 & 0 \\ \vdots & \vdots & \ddots & \ddots & \ddots & \vdots & \vdots \\ 0 & 0 & 0 & \ddots & e_\lambda & f_\lambda & 0 \\ 0 & 0 & 0 & \cdots & f_\lambda & e_\lambda & f_\lambda \\ 0 & 0 & 0 & \cdots & 0 & f_\lambda & d_\lambda \end{pmatrix}\,, \tag{4.29a}$$

with matrix entries

$$d_\lambda \equiv \coth\left(\frac{2\theta_\lambda}{k}\right) + \tanh\left(\frac{\theta_\lambda}{k}\right)\,; \qquad e_\lambda \equiv 2\coth\left(\frac{2\theta_\lambda}{k}\right)\,; \qquad f_\lambda \equiv -\mathrm{csch}\left(\frac{2\theta_\lambda}{k}\right)\,. \tag{4.29b}$$

In (4.29b), θ_λ is the principal branch of the square root function defined by

$$\theta_\lambda \equiv \theta_0\sqrt{1+\tau\lambda}\,, \qquad \theta_0 \equiv D^{-1/2}\,. \tag{4.29c}$$

Next, we substitute (4.21) and (4.25) into (4.24a). Since $h_{e\pm}(x_j) = H + o(1)$ as $\varepsilon \to 0$, we obtain the following problem for $\Phi(\xi)$, for $j = 1, \ldots, k$, where $\xi \equiv \sqrt{1+H_\pm}\,\varepsilon^{-1}(x - x_j)$:

$$b_j\left(\Phi'' - \Phi + pw^{p-1}\Phi\right) - (1+H_\pm)^{\gamma-1}\, w\,\eta(x_j) = \frac{\lambda b_j}{1+H_\pm}\,\Phi\,, \qquad -\infty < \xi < \infty\,, \tag{4.30}$$

with $\Phi(\xi) \to 0$ as $|\xi| \to \infty$. From (4.27) and (4.28), we obtain

$$\eta(x_j) = \frac{2\mu\, c_\pm^{2\gamma-2s-1}}{[1+\tau\lambda]^{1/2}}\left(\int_{-\infty}^{\infty} w\Phi\, d\xi\right)\left(\mathcal{B}_s^{-1}\boldsymbol{b}\right)_j\,. \tag{4.31}$$

To diagonalize (4.30), we must find the spectrum of the matrix eigenvalue problem

$$\mathcal{B}_s\boldsymbol{b} = \kappa\boldsymbol{b}\,. \tag{4.32}$$

The eigenpairs of $\mathcal{B}$ in (4.29) were calculated explicitly in Proposition 2 of [16] as

$$\kappa_j = e_\lambda + 2f_\lambda\cos\left(\frac{\pi(j-1)}{k}\right)\,, \quad j = 1, \ldots, k\,, \tag{4.33a}$$

$$\boldsymbol{b}_1^t = \frac{1}{\sqrt{k}}\,(1, \ldots, 1)\;; \quad b_{l,j} = \sqrt{\frac{2}{k}}\cos\left(\frac{\pi(j-1)}{k}\,(l-1/2)\right)\,, \quad j = 2, \ldots, k\,, \tag{4.33b}$$

with $\boldsymbol{b}_j^t = (b_{1,j}, \ldots, b_{k,j})$. From (4.28), the eigenvalues of $\mathcal{B}_s$ are simply translations of the eigenvalues of $\mathcal{B}$. Substituting (4.31) and (4.33a) into (4.30), we obtain the following nonlocal eigenvalue problem for the $O(1)$ eigenvalues of (4.24):

Proposition 4.3: *Assume that $0 < \varepsilon \ll 1$ and $\tau \geq 0$. Then, with $\Phi = \Phi(\xi)$, the $O(1)$ eigenvalues of (4.24) satisfy the nonlocal eigenvalue problem*

$$L_0\Phi - \chi_j w\int_{-\infty}^{\infty} w\Phi\, d\xi = \frac{\lambda}{1+H_\pm}\Phi\,, \quad -\infty < \xi < \infty\,; \qquad \Phi \to 0\,, \qquad \text{as} \quad |\xi| \to \infty\,. \tag{4.34a}$$

Here, L_0 is the local operator defined by $L_0\Phi \equiv \Phi'' - \Phi + pw^{p-1}\Phi$, and the multiplier χ_j, for $j = 1, \ldots, k$, is defined in terms of $\theta_\lambda = \theta_0\sqrt{1+\tau\lambda}$ and $\theta_0 = D^{-1/2}$ by

$$\chi_j \equiv \frac{\mu c_\pm^{4\gamma-2s-3}}{\sqrt{1+\tau\lambda}}\left[\tanh\left(\frac{\theta_\lambda}{k}\right) + \frac{(1-\cos[\pi(j-1)/k])}{\sinh(2\theta_\lambda/k)} + \frac{s\mu c_\pm^{4\gamma-2s-3} I_p}{2\sqrt{1+\tau\lambda}}\right]^{-1}\,. \tag{4.34b}$$

Eigenvalue problems of the form (4.34) also arise with regards to the stability of symmetric k-spike equilibria for the GM model (1.1) when $D = O(1)$ in (1.1b) (cf. [41]). We will restrict the analysis of (4.34) to the case where $\tau = 0$. The effect of the parameter τ for the GM model (1.1), as studied in detail in [41] for the case where $D = O(1)$, was to introduce the possibility of temporal oscillations in the heights of the spikes as τ is increased past some critical Hopf bifurcation value. The effect of nonzero τ on the model problem (4.1) is presumably similar to that for the GM model. When $\tau = 0$, (4.34b) reduces to

$$\chi_j \equiv \mu c_{\pm}^{4\gamma-2s-3}\left[\tanh\left(\frac{\theta_0}{k}\right) + \frac{(1-\cos\left[\pi(j-1)/k\right])}{\sinh\left(2\theta_0/k\right)} + \left(\frac{s\mu}{2}\right)c_{\pm}^{4\gamma-2s-3} I_p\right]^{-1}, \qquad j = 1,\ldots,k\,, \tag{4.35}$$

where $\theta_0 = D^{-1/2}$. In the analysis below, we need the following ordering principle for the multipliers χ_j, as is readily obtained from (4.35):

$$\chi_1 > \chi_2 > \ldots > \chi_k > 0\,. \tag{4.36}$$

To analyze the spectrum of (4.34) when $\tau = 0$ we use the following result:

Proposition 4.4: *Let $\alpha \geq 0$ and consider the nonlocal eigenvalue problem*

$$L_0\Phi - \alpha w\int_{-\infty}^{\infty} w\Phi\, d\xi = \sigma\Phi\,, \quad -\infty < \xi < \infty\,; \qquad \Phi \to 0 \quad \text{as} \quad |\xi| \to \infty\,. \tag{4.37}$$

Here $L_0\Phi \equiv \Phi'' - \Phi + pw^{p-1}\Phi$. Then, $\sigma \leq 0$ if and only if

$$\alpha > \alpha_c \equiv \left[\left(\frac{1}{p-1} - \frac{1}{4}\right) I_p\right]^{-1}, \qquad I_p \equiv \int_{-1}^{1} w^2\, d\xi\,. \tag{4.38}$$

To prove this result we first note that the nonlocal operator in (4.37) is self-adjoint, so that σ is real. Next we observe that $\sigma = 0$ with $\Phi = w'$ is an eigenpair of (4.37) for any $\alpha > 0$. To determine whether (4.37) has any positive eigenvalues, we need only look for eigenfunctions Φ that are even functions. To show this, we observe that the set of odd eigenfunctions of (4.37) and of L_0 coincide. However, it was proved in [22] that the local eigenvalue problem $L_0\phi_l = \nu\phi_l$ on the infinite line, has only one positive eigenvalue ν_0, and the corresponding eigenfunction ϕ_{l0} is an even function. Hence, in determining the stability of the equilibrium solutions we can assume that $\int_{-\infty}^{\infty} w\Phi\, d\xi \neq 0$. Then, from (4.37) we readily obtain that the eigenvalues of (4.37) are the roots of $\rho(\sigma) = 0$, where

$$\rho(\sigma) \equiv 1 - \alpha\int_{-\infty}^{\infty} w\left(L_0 - \sigma\right)^{-1} w\, d\xi\,. \tag{4.39}$$

By differentiating (4.39) we obtain

$$\rho'(\sigma) = -\alpha \int_{-\infty}^{\infty} \left[(L_0 - \sigma)^{-1} w \right]^2 d\xi \,. \tag{4.40}$$

Hence $\rho'(\sigma) < 0$ for $\alpha > 0$. Next, we calculate $\rho(0)$. Using the identity $L_0^{-1} w = \frac{w}{p-1} + \frac{1}{2}\xi w'$, we get

$$\rho(0) = 1 - \alpha \int_{-\infty}^{\infty} w L_0^{-1} w \, d\xi = 1 - \alpha \int_{-\infty}^{\infty} \left(\frac{w^2}{p-1} + \frac{1}{2}\xi w w' \right) d\xi = 1 - \alpha \left[\frac{1}{p-1} - \frac{1}{4} \right] \int_{-\infty}^{\infty} w^2 \, d\xi \,. \tag{4.41}$$

Let α_c be as given in (4.38). Thus, if $\alpha > \alpha_c$, we have $\rho(0) < 0$. Since $\rho'(\sigma) < 0$, this implies that $\rho(\sigma) < 0$ when $\alpha > \alpha_c$. Hence, (4.37) has no positive eigenvalues for $\alpha > \alpha_c$. Alternatively, suppose that $0 \le \alpha < \alpha_c$, so that $\rho(0) > 0$. Then, since $\rho'(\sigma) < 0$ and $\rho(\sigma) \to -\infty$ as $\sigma \to \nu_0^-$, where ν_0 is the unique positive eigenvalue of L_0, we conclude that there is a unique positive eigenvalue to (4.37). This completes the proof of Proposition 4.4.

We now use Proposition 4.4 to examine the stability of the two one-spike equilibrium solutions for (4.1) when $\tau = 0$. When $k = 1$, we get from (4.14), (4.35), and Proposition 4.4, that a one-spike solution is stable if and only if

$$\beta c_{\pm}^{4\gamma - 2s - 3} \ge \frac{2}{4\gamma - 2s - 1} \,. \tag{4.42}$$

Here β is defined in (4.14). From Lemma 4.1, we have $c_- < c_m < c_+$, where c_m satisfies (4.17). Therefore, from (4.42) we conclude that a_{e+} is stable, while a_{e-} is unstable. This leads to the following stability result:

Proposition 4.5: *Let p and s satisfy (4.16), and let $\tau = 0$. Suppose that $\mu < \mu_1$, where μ_1 is defined in (4.19). Then, for $\varepsilon \ll 1$, the one-spike equilibrium solution a_{e+}, h_{e+} given in Proposition 4.2 is stable on an $O(1)$ time-scale. Alternatively, the one-spike equilibrium solution a_{e-}, h_{e-} is unstable. When $\mu = \mu_1$, (4.34) has a zero eigenvalue of multiplicity two. One eigenfunction is the translation mode $\Phi = w'$, and the other eigenfunction Φ_d is a dimple eigenfunction given by*

$$\Phi_d(\xi) = -\left[\frac{w(\xi)}{p-1} + \frac{\xi}{2} w'(\xi) \right] . \tag{4.43}$$

To complete the proof of Proposition 4.5 we need only prove that Φ_d is an eigenfunction of (4.34) with zero eigenvalue when $k = 1$ and $\chi_1 = \alpha_c$. To verify that Φ_d is an eigenfunction, we need the identity

$$L_0 \left(\frac{w}{p-1} + \frac{1}{2}\xi w' \right) = w \,. \tag{4.44}$$

Then, from (4.37), (4.43), and (4.44), we calculate

$$L_0\Phi_d + \alpha_c w \int_{-\infty}^{\infty} \left[\frac{w^2}{p-1} + \frac{1}{2}\xi w w' \right] d\xi = -w + \alpha_c w \left(\frac{1}{p-1} - \frac{1}{4} \right) I_p = 0\,. \tag{4.45}$$

Hence Φ_d is an even eigenfunction of (4.34) with zero eigenvalue when $\mu = \mu_1$.

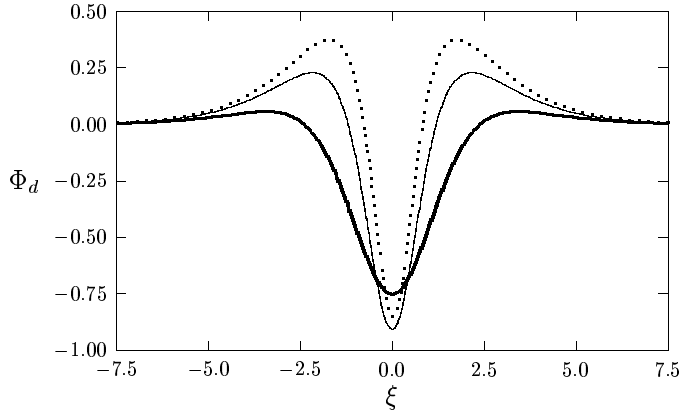

Figure 21: Plot of the dimple eigenfunction $\Phi_d(\xi)$ of (4.46) for $p = 2$ (heavy solid curve), $p = 3$ (solid curve), and $p = 4$ (dotted curve).

The function Φ_d has the *dimple property* of (1.4) as described in §1. We normalize Φ_d so that $\int_{-\infty}^{\infty} \Phi_d^2\, d\xi = 1$. Using (2.2b) for w, we calculate

$$\Phi_d(\xi) = -N \left(\cosh\left[\frac{(p-1)\xi}{2} \right] \right)^{-2/(p-1)} \left(\frac{1}{p-1} - \frac{\xi}{2} \tanh\left[\frac{(p-1)\xi}{2} \right] \right), \tag{4.46}$$

where $N > 0$ is a normalization constant. In Fig. 21, we plot Φ_d for $p = 2$, $p = 3$, and $p = 4$.

Next, we analyze the stability of a multi-spike solution with $k > 1$. From Proposition 4.4 and the ordering property (4.36), we observe that the smallest value of χ_j, for $j = 1, \ldots, k$, sets the stability threshold. Therefore, a k-spike solution will be stable with respect to the $O(1)$ eigenvalues if and only if $\chi_k > \alpha_c$, where χ_k and α_c are defined in (4.35) and (4.38), respectively. A little algebra shows that this inequality can be written as

$$\beta c_{\pm}^{4\gamma-2s-3} > \frac{2}{4\gamma - 2s - 1} \left[1 + \frac{(1 + \cos(\pi/k))}{2\sinh^2(\theta_0/k)} \right], \tag{4.47}$$

where β is defined in (4.14). Since $c_- < c_m$, where c_m is given in (4.17), we conclude from (4.47) that the solution branch corresponding to c_- is always unstable. This leads to the following result:

Proposition 4.6: *Let p and s satisfy (4.16), and let $\tau = 0$. Suppose that $0 < \mu < \mu_k$, where μ_k is defined in (4.19). Then, for $\varepsilon \ll 1$, the k-spike equilibrium solution a_{e-}, h_{e-} of Proposition 4.2 is unstable. Alternatively, the k-spike equilibrium solution a_{e+}, h_{e+} given in Proposition 4.2 is stable on an $O(1)$ time-scale if and only if (4.47) holds.*

The stability condition (4.47) does not hold near the fold point where we have $\beta c_\pm^{4\gamma-2s-3} = 2/(4\gamma-2s-1)$. In the plots Fig. 19(a) and Fig. 19(b), where $p = 2$ and $s = 0$, the unstable portions of the solution branches where (4.47) does not hold are given by the dotted lines. From Lemma 4.1, we have $\beta c_+^{4\gamma-2s-3} < 1$. Therefore, from (4.47) we conclude that the entire upper branch is unstable when D is such that

$$\sinh^2\left(\frac{\theta_0}{k}\right) < \frac{[1+\cos(\pi/k)]}{4\gamma-2s-3}\,. \tag{4.48}$$

Setting $\theta_0 = D^{-1/2}$, this yields that the entire upper branch is unstable when $D > D_k$, where

$$D_k \equiv \left[k\ln\left(\sqrt{\delta_k}+\sqrt{\delta_k+1}\right)\right]^{-2}\,, \qquad \delta_k \equiv \frac{[1+\cos(\pi/k)]}{4\gamma-2s-3}\,. \tag{4.49}$$

To illustrate this result, consider the case where $p = 2$ and $s = 0$. Then, from (4.49) we calculate $D_2 = 0.322$ and $D_3 = 0.104$. Hence, in Fig. 19(a), where $D = 0.25$, we obtain that the entire upper branch for $k = 3$ is unstable.

Notice also that when $D \to 0$ with k fixed, we have $\sinh(\theta_0/k) \to \infty$. Therefore, in this limit, where the lining-up property of the fold points occur, the stability condition (4.49) reduces approximately to $\beta c_\pm^{4\gamma-2s-3} \geq 2/(4\gamma-2s-1)$. From (4.17), this implies that when D is small, almost all of the upper branch for a k-spike equilibria will be stable, whereas the entire lower branch is unstable. This behavior was seen in Fig. 19(b) when $p = 2$, $s = 0$, and $D = 0.025$.

4.3 Numerical Computations

For (4.1), we have shown that k-spike equilibria have a saddle-node bifurcation structure with an approximate *lining-up property*. All of the other pulse-splitting conditions of [11], listed in §1, are found to hold when D is small and $\tau = 0$. However, the *multi-bump transition condition* of §1 does not hold. We now perform a few numerical experiments using the NAG routine D03PCF (cf. [29]) to see whether pulse-splitting occurs.

Experiment 4.1: We consider a one-spike solution centered at the origin for the parameter values $D = 0.025$, $\varepsilon = 0.02$, $k = 1$, $\tau = 0.001$, and $(p, s) = (2, 0)$. The initial condition for the full

numerical solution of (4.1) is the one-spike profile a_{e+} and h_{e+} of Proposition 4.2. Recall that, for this parameter set, the bifurcation diagram of k-spike equilibria is shown in Fig. 19(b), and the saddle-node values for μ_k^{-1} are given in the second row of Table 3, with $\mu_1 = 1/7.79 \approx 0.128$. In the numerical computations, we let $\mu = \mu(t)$ have a slow time dependence of the form

$$\mu = 0.1\,(1 + \delta \max(t-5,0))\ , \quad \delta = 0.01\,. \tag{4.50}$$

Therefore, as t increases, μ eventually exceeds the saddle-node value $\mu_1 \approx 0.128$, and we lose the existence of a steady-state spike solution. Using (4.50), this transition occurs when $t \approx 33$. By solving (4.1) with (4.50) numerically, we show in Fig. 22(a) that the spike does not exhibit pulse-splitting behavior beyond the saddle-node bifurcation value, but instead is annihilated. In Fig. 22(b) we plot the height of the spike versus t showing the collapse behavior.

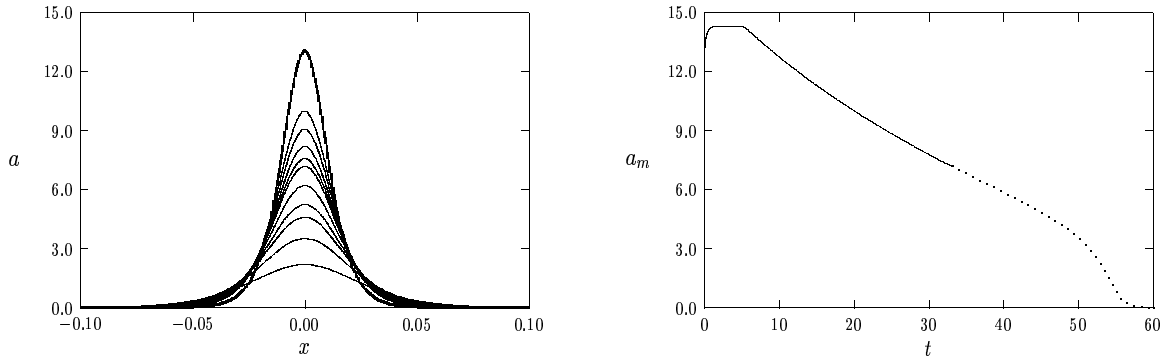

(a) $a(x,t)$ (b) $a_m(t)$

Figure 22: Experiment 4.1: numerical solution of (4.1) for $D = 0.025$, $\varepsilon = 0.02$, $(p,s) = (2,0)$, $k = 1$, $\tau = 0.001$, and (4.50) for μ. Left figure: a versus x at $t = 0$ (heavy solid curve) and at $t = 20, 24, 28, 31, 33, 38, 43, 46, 50, 53$. Right figure: $a_m(t) \equiv a(0,t)$ versus t. The dotted portion of this curve is where there is no longer a steady-state spike solution.

Experiment 4.2: We perform a similar experiment for the different parameter set $D = 0.025$, $\varepsilon = 0.02$, $k = 1$, $\tau = 0.001$, and $(p,s) = (3,-1)$. The initial condition for (4.1) is the one-spike profile a_{e+} and h_{e+} of Proposition 4.2, and the saddle-node values of μ_k^{-1} are given in the fourth row of Table 3, with $\mu_1 = 1/5.2 \approx 0.192$. We let $\mu = \mu(t)$ have a slow time dependence of the form

$$\mu = 0.15\,(1 + \delta \max(t-5,0))\ , \qquad \delta = 0.01\,, \tag{4.51}$$

so that there is no steady-state spike solution for $t \geq 31$. With $p = 3$, we see from Fig. 21 that the dimple-shaped eigenfunction is significantly more pronounced than it was for Experiment 4.1 where $p = 2$. However, by solving (4.1) with (4.51) numerically, we show in Fig. 23(a) that the spike again does not exhibit pulse-splitting behavior beyond the saddle-node bifurcation value. In Fig. 23(b) we show that the spike amplitude again decreases to zero on the range $\mu > \mu_1$.

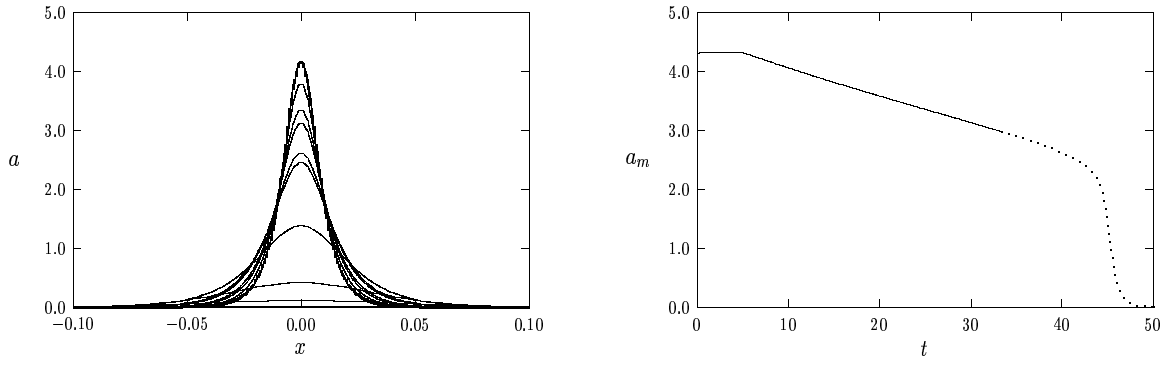

(a) $a(x,t)$ (b) $a_m(t)$

Figure 23: Experiment 4.2: numerical solution of (4.1) for $D = 0.025$, $\varepsilon = 0.02$, $(p,s) = (3,-1)$, $k = 1$, $\tau = 0.001$, and (4.51) for μ. Left figure: a versus x at $t = 0$ (heavy solid curve) and at $t = 15, 25, 30, 40, 42, 45, 46, 47$. Right figure: $a_m(t) \equiv a(0,t)$ versus t. The dotted portion of this curve is where there is no longer a steady-state spike solution.

We have performed many other numerical experiments similar to Experiments 4.1 and 4.2 to try to exhibit pulse-splitting behavior. However, we have had no success. These experiments include explorations with other parameter sets, and the effect of decreasing the control parameter δ in (4.50) and (4.51) by several decades. Although this does not categorically prove that pulse-splitting behavior does not occur for (4.1) for parameters slightly beyond the saddle-node value, it does suggest that this behavior is not a robust phenomena for (4.1). Two possibilities for the likely non-existence of pulse-splitting for (4.1) are that the *multi-bump transition condition* of §1 does not hold, and that the nesting property of k-spike equilibria is such that $\mu_1 > \mu_k$ for any $k > 1$. Therefore, if $\mu > \mu_1$, so that a one-spike solution does not exist, then there are also no equilibrium solutions with more than one spike. This nesting property associated with the approximate lining-up criterion is qualitatively different than that for the GS model discussed in §3 (see Fig. 2(a)).

Despite this obvious difference in the nesting behavior of saddle-node equilibria, one might have predicted that a one-spike solution for (4.1) undergoes a transient splitting process, whereby a one-spike profile splits into two spikes as μ is increased past μ_1, but with these two spikes being subsequently annihilated at later times.

Experiment 4.3: Finally, we perform an experiment suggested by the stability information on the bifurcation diagram of Fig. 19(a). We take the parameter set $D = 0.25$, $\varepsilon = 0.02$, $k = 2$, $\tau = 0.001$, and $(p, s) = (2, 0)$. The slowly varying function $\mu(t)$ is chosen to be

$$\mu = 0.06\,(1 + \delta \max(t - 5, 0))\;, \quad \delta = 0.01\,. \tag{4.52}$$

The initial condition for (4.1) is the two-spike equilibrium of Proposition 4.2. From the first row of Table 3 we observe that the two-spike equilibrium does not exist when $\mu > 0.098$. From (4.47) and Proposition 4.6, the upper branch with $k = 2$ in Fig. 19(a) is unstable on the range $0.070 < \mu < 0.098$. Hence, when $t \approx 21$, there will be a transition where the quasi-static two-spike solution loses its stability. In Fig. 24(a) and Fig. 24(b) we plot the numerical solution for $a(x, t)$ near the first and second spikes, respectively, at later times. The amplitudes of the two spikes are shown in Fig. 25. It is found that both spikes are annihilated once the stability threshold for μ is exceeded. Since the initial data is symmetric, the spike that gets annihilated first depends on the amplification of small symmetry-breaking discretization errors of the numerical scheme.

5 Pulse-Splitting Criteria: a Semi-Strong RD Model II

In this section we consider another model reaction-diffusion system of the class (1.5) in the semi-strong interaction limit. This system is given by

$$a_t = \varepsilon^2 a_{xx} + a - ah + a^3\,, \qquad -1 < x < 1\,, \quad t > 0\,, \tag{5.1a}$$

$$\tau h_t = D h_{xx} - h + 2\varepsilon^{-1}\beta a^2\,, \qquad -1 < x < 1\,, \quad t > 0\,, \tag{5.1b}$$

$$a_x(\pm 1, t) = h_x(\pm 1, t) = 0\,; \qquad a(x, 0) = a_0(x)\,, \qquad h(x, 0) = h_0(x)\,. \tag{5.1c}$$

In (5.1), $0 < \varepsilon \ll 1$, $D > 0$, $\beta > 0$, and $\tau \geq 0$, are constants, with $D = O(1)$ as $\varepsilon \to 0$. This system is very similar to (4.1), with the main difference being the different sign of the coefficient of a in the reaction kinetics of (5.1a) and (4.1a). In the shadow limit where $D \gg 1$ and $\tau \ll 1$, (5.1) reduces to the following nonlocal Ginzburg-Landau model:

$$a_t = \varepsilon^2 a_{xx} - \left(\beta\varepsilon^{-1}\int_{-1}^{1} a^2\,dx - 1\right) a + a^3\,, \qquad -1 < x < 1\,; \quad a_x(\pm 1) = 0\,. \tag{5.2}$$

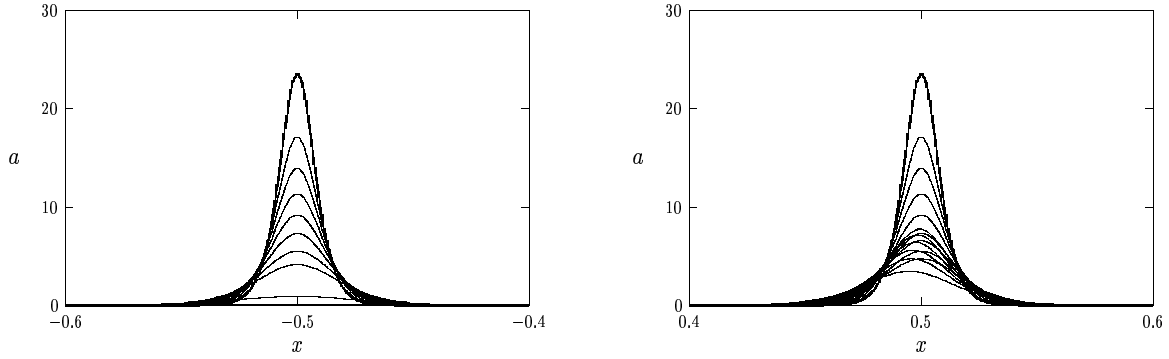

(a) $a(x,t)$ near x_1 (b) $a(x,t)$ near x_2

Figure 24: Experiment 4.3: numerical solution of (4.1) with $D = 0.25$, $\varepsilon = 0.02$, $(p,s) = (2,0)$, $k = 2$, $\tau = 0.001$, and (4.52) for μ. Left figure: a versus x near x_1 at $t = 0$ (heavy solid curve) and at $t = 10, 20, 30, 40, 50, 60, 70, 80$. This spike is annihilated first. Right figure: plots of a versus x near x_2 at $t = 0$ (heavy solid curve) and at $t = 10, 20, 30, 40, 50, 60, 70, 80, 90, 100, 105$.

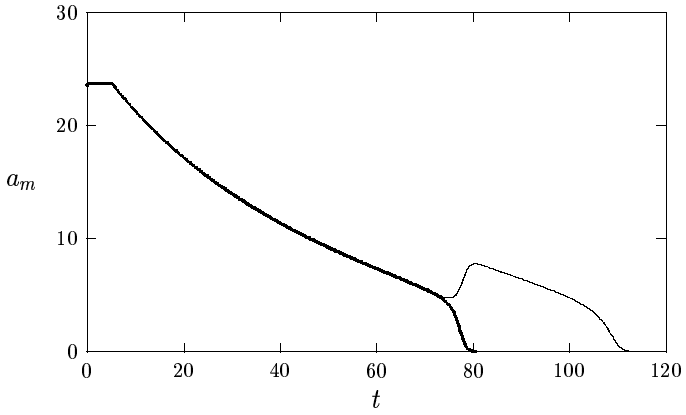

Figure 25: Experiment 4.3: with the parameters of Fig. 24, we plot a_{m1} (heavy solid curve) and a_{m2} (solid curve) versus t, representing the heights of the two spikes, with $a_{m1}(0) = a(-0.5, 0)$ and $a_{m2}(0) = a(0.5, 0)$. The spike a_{m1} is annihilated first, followed eventually by the second spike.

This limiting model, which arises in asymptotic theories of certain convection processes (cf. [23], [38]), was studied in [33] and [43].

For (5.1), we construct k-spike equilibria and we analyze their stability properties. The analysis shows that all of the pulse-splitting criteria of [11], listed in §1, again hold in an approximate sense, with the exception of the *multi-bump transition condition*. Some numerical experiments are then performed to determine whether pulse-splitting occurs. Since the study of spike solutions for (5.1) is very similar to that for (4.1), we will only give the main results of the analysis.

By asymptotically constructing k-spike equilibria for $\varepsilon \ll 1$ in a similar way as in §4.1, we obtain the following result:

Proposition 5.1: *Let $0 < \varepsilon \ll 1$, and and define β_k by*

$$\beta_k = (2\theta_0)^{-1} \tanh(\theta_0/k) \ . \tag{5.3}$$

For $\beta > \beta_k$, we further define $\omega > 1$ and $c_\pm$ by

$$\omega = \beta/\beta_k \,, \qquad c_\pm = \omega \pm \sqrt{\omega^2 - 1} \,. \tag{5.4}$$

Then, for $0 < \beta < \beta_k$ there are no symmetric k-spike equilibria to (5.1). For $\beta > \beta_k$, there are exactly two symmetric k-spike equilibria to (5.1) given asymptotically by

$$a_{e\pm}(x) \sim c_\pm \sum_{j=1}^{k} w\left[c_\pm \, \varepsilon^{-1}(x - x_j)\right] \ , \qquad w(\xi) \equiv \sqrt{2}\,\mathrm{sech}\xi \,, \tag{5.5a}$$

$$h_{e\pm}(x) \sim 8\beta c_\pm \sum_{j=1}^{k} G_0(x; x_j) \,, \quad |x - x_i| \gg O(\varepsilon) \,, \quad x_i = -1 + \frac{(2i-1)}{k} \,. \tag{5.5b}$$

Here G_0 is the Green's function satisfying (4.11).

In the usual way, we define a norm $|a|_2$ by

$$|a|_2 \equiv \left(\sum_{j=1}^{k} \left[a_{e\pm}(x_j)\right]^2 \right)^{1/2} \sim c_\pm w(0)\sqrt{k} = \sqrt{2k}\, c_\pm \,. \tag{5.6}$$

In Fig. 26(a) we plot $|a|_2$ versus β when $D = 0.1$ for $k = 1, 2, 3$. A similar plot is shown in Fig. 26(b) for $D = 0.25$. The top and bottom portions of each of these solution branches corresponds to a_{e+} and a_{e-}, respectively. When $\tau = 0$, the segments of these branches that are unstable on an $O(1)$ time-scale correspond to the dotted lines. Stable segments correspond to the solid lines. Notice that we have an approximate lining-up property of saddle-node equilibria when $D \ll 1$.

However, in contrast to the behavior for (4.1), the nesting property of equilibria is now such that the non-existence of a one-spike equilibrium solution does not imply the non-existence of multi-spike equilibria.

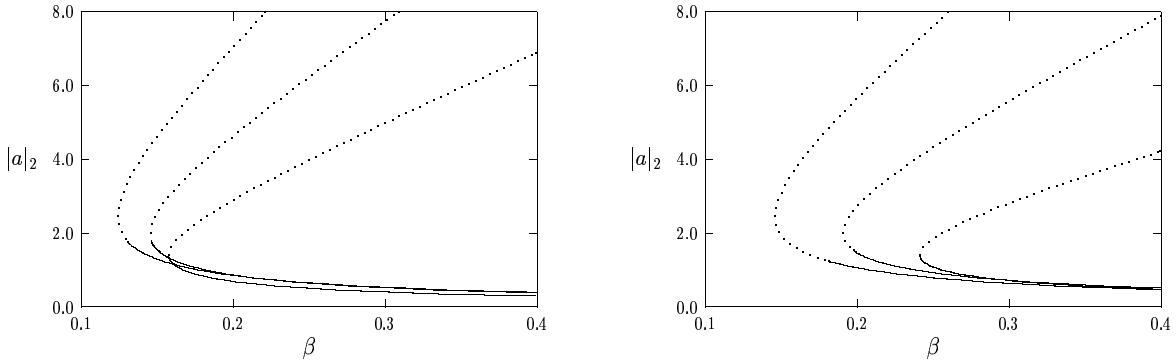

(a) $D = 0.1$ (b) $D = 0.25$

Figure 26: The norm $|a|_2$, defined in (5.6), versus β for $k = 1, 2, 3$ for $D = 0.1$ (left figure) and $D = 0.25$ (right figure). The portions of the branches that are unstable on an $O(1)$ time-scale correspond to the dotted lines. The β value at the fold point in these figures decrease with increasing k.

The stability of k-spike solutions can be analyzed in a similar way as in §4.2. In place of Proposition 4.3, we obtain the following nonlocal eigenvalue problem:

Proposition 5.2: *Assume that $0 < \varepsilon \ll 1$ and $\tau \geq 0$. Then, with $\Phi = \Phi(\xi)$, a k-spike equilibrium for (5.1) is stable on an $O(1)$ time scale, if the following nonlocal eigenvalue problem has no spectra in $Re(\lambda) > 0$:*

$$L_0\Phi - \chi_j w \int_{-\infty}^{\infty} w\Phi \, d\xi = \frac{\lambda}{c_{\pm}^2}\Phi\,, \quad -\infty < \xi < \infty\,; \qquad \Phi \to 0\,, \qquad \text{as} \quad |\xi| \to \infty\,. \tag{5.7a}$$

Here, L_0 is the local operator defined by $L_0\Phi \equiv \Phi'' - \Phi + 3w^2\Phi$, and the multiplier χ_j, for $j = 1, \ldots, k$, is defined in terms of $\theta_\lambda \equiv \theta_0\sqrt{1+\tau\lambda}$ and $\theta_0 \equiv D^{-1/2}$ by

$$\chi_j \equiv \frac{2\beta}{c_{\pm}\left[(1+\tau\lambda)D\right]^{1/2}}\left[\tanh\left(\frac{\theta_\lambda}{k}\right) + \frac{(1-\cos\left[\pi(j-1)/k\right])}{\sinh\left(2\theta_\lambda/k\right)}\right]^{-1}\,, \qquad j = 1, \ldots, k\,. \tag{5.7b}$$

Next, Proposition 4.4 is used to determine the stability of k-spike equilibria when $\tau = 0$. In this way, we obtain the following explicit stability result:

Proposition 5.3: *Let $\varepsilon \ll 1$ and $\tau = 0$. Suppose that $\beta > \beta_1$. Then, the one-spike equilibrium solution a_{e+}, h_{e+} given in Proposition 5.1 is unstable, while the equilibrium a_{e-}, h_{e-} is stable on an $O(1)$ time scale. When $\beta = \beta_1$, there is a double-zero eigenvalue, with eigenfunctions $\Phi = w'$, and $\Phi = \Phi_d$. Here Φ_d is the dimple eigenfunction of (4.46) with $p = 3$ shown in Fig. 21. For $k > 1$, the multi-spike solution a_{e+}, h_{e+} of Proposition 5.1 is unstable. Alternatively, the multi-spike equilibrium a_{e-}, h_{e-} is stable on an $O(1)$ time-scale if and only if*

$$\left[1 - \sqrt{1 - \frac{1}{\omega^2}}\right]^{-1} \geq 1 + \frac{[1 + \cos(\pi/k)]}{2\sinh^2(\theta_0/k)}, \qquad \theta_0 \equiv D^{-1/2}. \tag{5.8}$$

Here ω is defined in terms of β by (5.4). At each fold point, for $k \geq 1$, the function Φ_d of (4.46) with $p = 3$ is a dimple eigenfunction corresponding to a zero eigenvalue.

5.1 Numerical Computations

We now perform some numerical experiments to see if pulse-splitting behavior occurs for (5.1).

Experiment 5.1: We consider a one-spike solution centered at the origin for the parameter values $D = 10$, $\varepsilon = 0.02$, and $\tau = 0.001$. The initial condition for the full numerical solution of (5.1) is the one-spike profile a_{e-} and h_{e-} of Proposition 5.1. From (5.3), we see that there is no equilibrium one-spike solution when $0 < \beta < \beta_1 = 0.484$. To see if pulse-splitting occurs just below the fold point, we solve (5.1) numerically for a slowly varying function $\beta(t)$ given by

$$\beta = \begin{cases} 0.60\,(1 - \delta \max(t - 5, 0))\,, & 0 < t < 48.33\,, \\ 0.47\,, & t > 48.33\,, \end{cases} \tag{5.9}$$

with $\delta = 0.005$. From (5.9), it follows that, as t increases, β eventually decreases below β_1 at $t = 43.66$, and we lose the existence of an equilibrium spike solution. By solving (5.1) with (5.9) numerically, we show in Fig. 27(a) that the spike does not exhibit pulse-splitting behavior below the saddle-node value, but instead appears to blow-up in finite time. In Fig. 27(b) we plot the height of the spike versus t showing the dramatic increase in the spike amplitude when β is below the fold-point value.

Experiment 5.2: Next, we consider a one-spike solution centered at the origin for the parameter values $D = 0.1$, $\varepsilon = 0.02$, and $\tau = 0.001$. Our initial condition is again the one-spike equilibrium solution a_{e-} and h_{e-} of Proposition 5.1. From (5.3), the one-spike and two-spike equilibrium

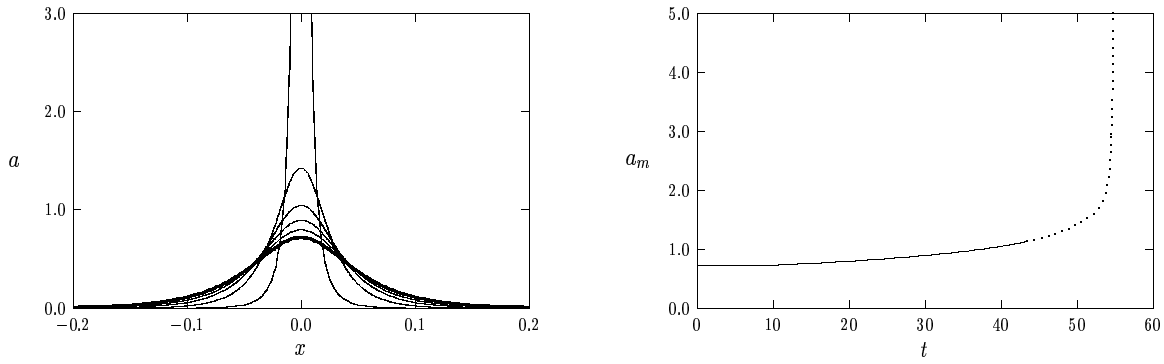

(a) $a(x,t)$ near $x = 0$ (b) $a_m = a(0,t)$

Figure 27: Experiment 5.1: numerical solution of (5.1) with $\varepsilon = 0.02$, $D = 10$, $\tau = 0.001$, and for $\delta = 0.005$ in (5.9). Left figure: a versus x near $x = 0$ at $t = 0$ (heavy solid curve) and at $t = 10, 20, 30, 40, 50, 54.65$. Right figure: the spike amplitude. There is no equilibrium one-spike solution on the dotted portion of this curve. Finite-time blow-up appears to occur near $t = 54.8$.

solution branches exist for $\beta > \beta_1 = 0.158$ and $\beta > \beta_2 = 0.145$, respectively. From (5.8) and Fig. 26(a), the lower branch for a two-spike solution is stable for $\beta > 0.146$. To see if pulse-splitting occurs just below the fold point β_1, we solve (5.1) numerically for a slowly varying function $\beta(t)$ given by

$$\beta = \begin{cases} 0.17\,(1 - \delta \max(t-5,0)) \,, & 0 < t < t_{\rm sw} \,, \\ 0.14 \,, & t > t_{\rm sw} \,. \end{cases} \tag{5.10}$$

For Experiment 5.2a we take $\delta = 0.01$, so that $t_{\rm sw} = 22.65$. Notice that $\beta < \beta_1$ when $t > 12.35$. In Fig. 28 we plot the numerically computed a versus x at different times. Pulse-splitting is not observed, but instead new local maxima are created on either side of the spike at later times. The final equilibrium state for a is spatially uniform.

In Experiment 5.2b we take the parameter values as above, but we now choose the slightly larger value $\sigma = 0.011$, so that $t_{\rm sw} = 13.0$. In Fig. 29(a) we plot a versus x at three different times, and in Fig. 29(b) we observe what appears to be finite-time blow-up for the spike located at the origin when β is slightly below the existence threshold β_1.

Therefore, for (5.1) we do not observe pulse-splitting behavior when β is slightly below the saddle-node value, but instead we observe the possibility of finite-time blow-up.

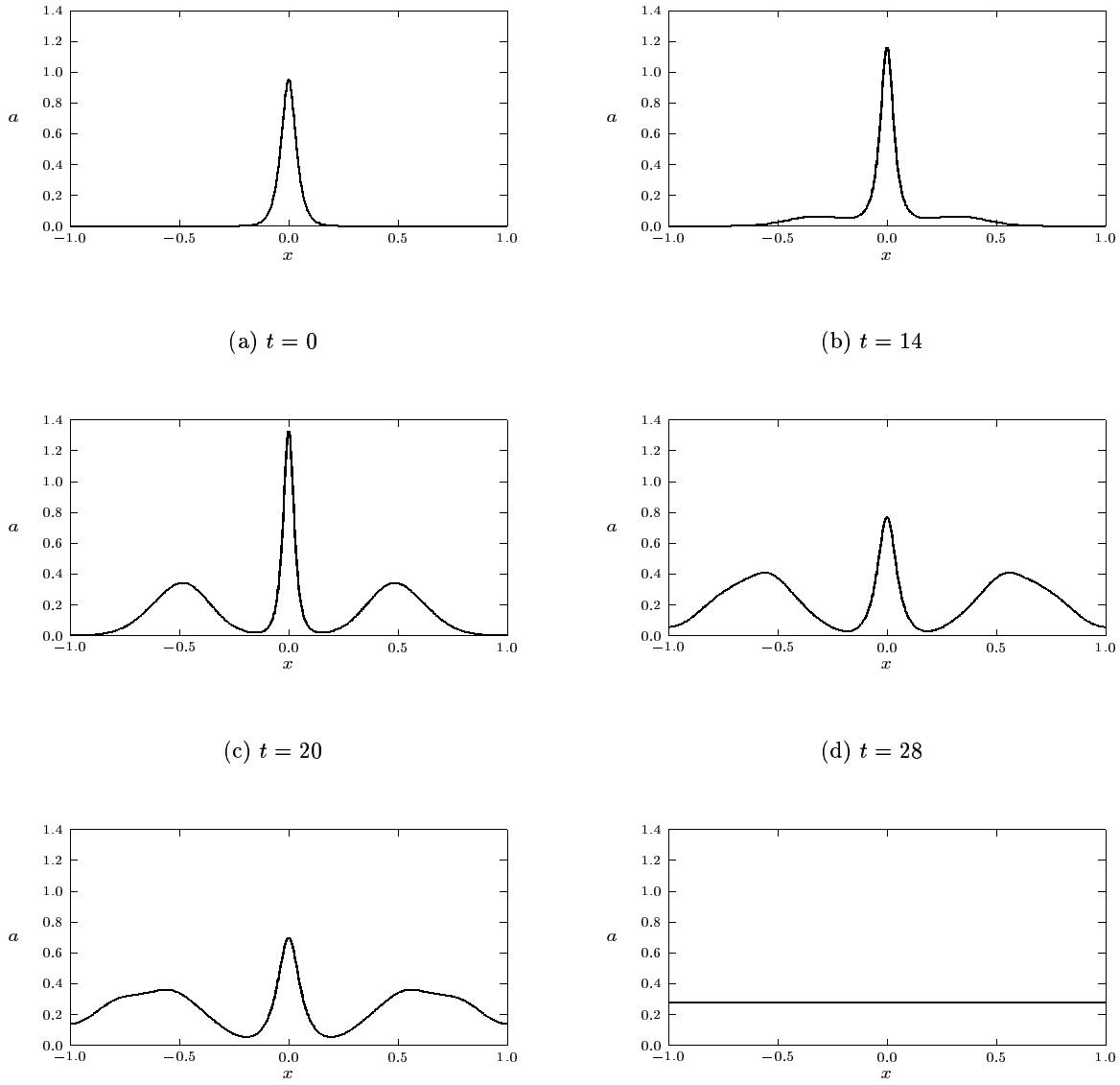

(a) $t = 0$

(b) $t = 14$

(c) $t = 20$

(d) $t = 28$

(e) $t = 33$

(f) $t = 200$

Figure 28: Experiment 5.2a: numerical solution for a versus x from (5.1) at different times. The parameter values are $\varepsilon = 0.02$, $D = 0.1$, $\tau = 0.001$, and β is given by (5.10) with $\delta = 0.01$. There is no finite-time blow-up.

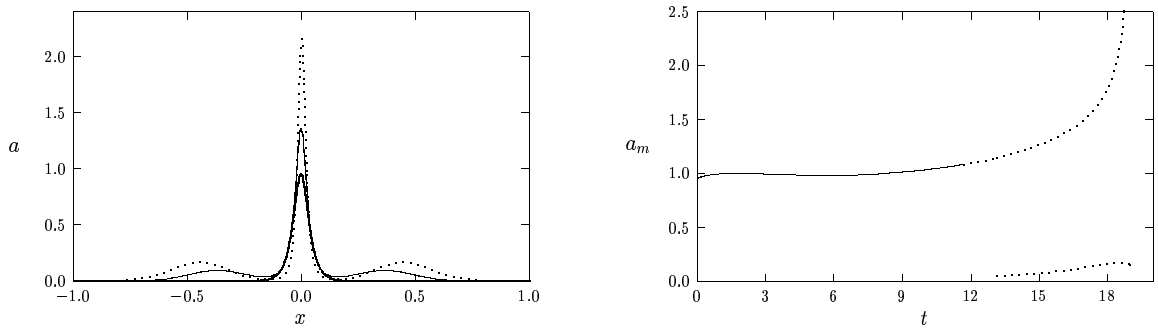

(a) $a(x,t)$ (b) spike amplitude

Figure 29: Experiment 5.2b: numerical solution of (5.1) with $\varepsilon = 0.02$, $D = 0.1$, $\tau = 0.001$, and for $\delta = 0.011$ in (5.10). Left figure: a versus x at $t = 0$ (heavy solid curve), $t = 16$ (solid curve), and $t = 18.5$ (dotted curve). Right figure: the spike amplitude at $x = 0$ (larger value), and the amplitude of the newly created bumps. The dotted portion of these curves are where there is no longer an equilibrium one-spike solution. Finite-time blow-up appears to occur near $t = 19.0$.

Although it is beyond our scope here to give a precise quantitative explanation of the solution behavior seen in Experiments 5.1 and 5.2, qualitatively we suggest that this behavior is closely related to the sign of the coefficient a in (5.1a). Notice that if $h - 1 < 0$ on some interval in x, then this term is destabilizing with respect to the background state $a = 0$. For D large, such as in Experiment 5.1, h decreases slowly away from $x = 0$, and so the condition $h > 1$ is easily satisfied on most of the interval, except possibly near the core of the spike. Hence, the background state $a = 0$ is stable, and so when β decreases below β_1, there is no possibility to prevent finite-time blow-up by creating new bumps to suppress the growth of the spike at $x = 0$. However, when D is small, such as in Experiment 5.2, h decays quickly away from $x = 0$, and so $h < 1$ for most of the interval. This leads to an instability of the background state $a = 0$ away from the spike, and is probably the mechanism by which the new bumps in a are formed in Fig. 28 and Fig. 29. If these bumps can be created *before* β dips below the existence threshold β_1, finite-time blow-up is prevented. This will occur when δ in (5.10) is sufficiently small, so that β decreases sufficiently slowly. This is presumably the mechanism at work in Experiment 5.2a. Alternatively, we suggest that if β decreases below β_1 before the new bumps are sufficiently well-formed, such as shown in Experiment 5.2b where δ is slightly larger than in Experiment 5.2a (see in particular Fig. 29(b)),

then finite-time blow-up can occur.

6 Discussion

There are several open problems that should be explored. The first problem is to determine under what general conditions can one guarantee analytically, in an apriori sense, that the core problem for a one-spike solution to a reaction-diffusion system in the weak interaction region will have a saddle-node bifurcation, a dimple eigenfunction at the fold point, and satisfy the *multi-bump transition condition*. Are these conditions generic to a wide class of systems, or is some special structure required? The second problem is to determine whether it is possible to construct a reaction-diffusion system in the semi-strong interaction regime, for which both components can be asymptotically decoupled in the core region, that exhibits robust pulse-splitting behavior near the fold point. For such systems, we have not been able to find an example where the *multi-bump transition condition* of §1 holds. Finally, for a one-spot initial data, it would be interesting to identify and classify mechanisms that lead to spot-splitting behavior in two space dimensions. Our preliminary work indicates that there are two such mechanisms.

Acknowledgements

T. K. was supported by a PGS-B graduate scholarship from NSERC (Canada). M. J. W. thanks NSERC (Canada) for their support under grant 81541. J. W. thanks the support of RGC of Hong Kong and a direct grant from CUHK. The use of the computer facilities from the University of Washington Applied Math group is most gratefully acknowledged.

References

[1] E. Anderson et al. *LAPACK User's Guide: Third Edition*, SIAM Publications (1999).

[2] U. Ascher, R. Christiansen, R. Russell, *Collocation Software for Boundary Value ODE's*, Math. Comp., **33**, (1979), pp. 659-679.

[3] M. Del Pino, M. Kowalczyk, X. Chen, *The Gierer Meinhardt System: The Breaking of Homoclinics and Multi-Bump Ground States*, Commun. Contemp. Math., 3, No. 3, (2001), pp. 419-439.

[4] A. Doelman, W. Eckhaus, T. J. Kaper, *Slowly Modulated Two-Pulse Solutions in the Gray-Scott Model I: Asymptotic Construction and Stability*, SIAM J. Appl. Math., **61**, No. 3, (2000), pp. 1080-1102.

[5] A. Doelman, W. Eckhaus, T. J. Kaper, *Slowly Modulated Two-Pulse Solutions in the Gray-Scott Model II: Geometric Theory, Bifurcations, and Splitting Dynamics*, SIAM J. Appl. Math., **61**, No. 6, (2000), pp. 2036-2061.

[6] A. Doelman, R. A. Gardner, T. J. Kaper, *Stability Analysis of Singular Patterns in the 1D Gray-Scott Model: A Matched Asymptotics Approach*, Physica D, **122**, (1998), pp. 1-36.

[7] A. Doelman, R. A. Gardner, T. Kaper, *A Stability Index Analysis of 1-D Patterns of the Gray Scott Model*, Memoirs of the AMS, **155**, No. 737, (2002).

[8] A. Doelman, R. A. Gardner, T. Kaper, *Large Stable Pulse Solutions in Reaction-Diffusion Equations*, Indiana U. Math. Journ., Vol. 50, No. 1, (2001), pp. 443-507.

[9] A. Doelman, T. J. Kaper, P. Zegeling, *Pattern Formation in the One-Dimensional Gray-Scott Model*, Nonlinearity, **10**, (1997), pp. 523-563.

[10] A. Doelman, H. van der Ploeg, *Homoclinic Stripe Patterns*, SIAM J. Appl. Dyn. Systems, **1**, No. 1, (2002), pp. 65-104.

[11] S. Ei, Y. Nishiura, K. Ueda, 2^n *Splitting or Edge Splitting?: A Manner of Splitting in Dissipative Systems*, Japan. J. Indust. Appl. Math., **18**, (2001), pp. 181-205.

[12] T. Erneux, E. L. Reiss, L. J. Holden, M. Georgiou, *Slow Passage Through Bifurcation and Limit Points. Asymptotic Theory and Applications*, Dynamic Bifurcations (Luminy 1990), pp. 14-28, Lecture Notes in Math., **1493**, Springer, Berlin, (1991).

[13] A. Gierer, H. Meinhardt, *A Theory of Biological Pattern Formation*, Kybernetik, **12**, (1972), pp. 30–39.

[14] G. Goldsztein, F. Broner, S. H. Strogatz, *Dynamical Hysteresis Without Static Hysteresis: Scaling Laws and Asymptotic Expansions*, SIAM J. Appl. Math., **57**, No. 4, (1997), pp. 1163-1187.

[15] P. Gray, S. K. Scott, *Autocatalytic Reactions in the Isothermal, Continuous Stirred Tank Reactor: Oscillations and Instabilities in the System* $A + 2B \to 3B$, $B \to C$, Chem. Eng. Sci. **39**, (1984), pp. 1087-1097.

[16] D. Iron, M. J. Ward, J. Wei, *The Stability of Spike Solutions to the One-Dimensional Gierer-Meinhardt Model*, Physica D, **150**, No. 1-2, (2001), pp. 25-62.

[17] D. Iron, M. J. Ward, *The Dynamics of Multi-Spike Solutions to the One-Dimensional Gierer-Meinhardt Model*, SIAM J. Appl. Math., **62**, No. 6, (2002), pp. 1924-1951. (electronic)

[18] H. B. Keller, *Lectures on Numerical Methods in Bifurcation Problems*, Tata Institute of Fundamental Research Lectures on Mathematics and Physics, **79**, published for the Tata Institute, Bombay, by Springer-Verlag, Berlin, (1987).

[19] T. Kolokolnikov, M. Ward, J. Wei, *The Stability of Spike Equilibria in the One-Dimensional Gray-Scott Model: The Low Feed-Rate Regime*, submitted, Memoirs of the AMS, (2003).

[20] T. Kolokolnikov, M. Ward, J. Wei, *The Stability of Spike Equilibria in the One-Dimensional Gray-Scott Model: The Pulse-Splitting Regime*, submitted, Physica D, (2003).

[21] K. J. Lee, W. D. McCormick, J. E. Pearson, H. L. Swinney, *Experimental Observation of Self-Replicating Spots in a Reaction-Diffusion System*, Nature, **369**, (1994), pp. 215-218.

[22] C. S. Lin, W. M. Ni, I. Takagi, *Large Amplitude Stationary Solutions to a Chemotaxis System*, J. Diff. Eq., **72**, No. 1, (1988), pp. 1-27.

[23] P. C. Matthews, S. M. Cox, *Pattern Formation with a Conservation Law*, Nonlinearity, **13**, No. 4, (2000), pp. 1293-1320.

[24] H. Meinhardt, *Models of Biological Pattern Formation*, Academic Press, London, (1982).

[25] H. Meinhardt, *The Algorithmic Beauty of Sea Shells*, The Virtual Laboratory, Springer-Verlag, Berlin, (1995).

[26] C. Muratov, V. V. Osipov, *Traveling Spike Auto-Solitons in the Gray-Scott Model*, Physica D, **155**, No. 1-2, (2001), pp. 112-131.

[27] C. Muratov, V. V. Osipov, *Stability of the Static Spike Autosolitons in the Gray-Scott Model*, SIAM J. Appl. Math., **62**, No. 5, (2002), pp. 1463-1487.

[28] C. Muratov, V. V. Osipov, *Static Spike Autosolitons in the Gray-Scott Model*, J. Phys. A: Math Gen. **33**, (2000), pp. 8893-8916.

[29] NAG Fortran library Mark 17, routine D03PCF, Numerical Algorithms Group Ltd., Oxford, United Kingdom (1995).

[30] Y. Nishiura, *Far-From-Equilibrium Dynamics*, Translations of Mathematical Monographs, Vol. 209, AMS publications, Providence, Rhode Island, (2002).

[31] Y. Nishiura, D. Ueyama, *A Skeleton Structure of Self-Replicating Dynamics*, Physica D, **130**, (1999), pp. 73-104.

[32] Y. Nishiura, D. Ueyama, *Spatial-Temporal Chaos for the Gray-Scott Model*, Physica D, **150**, (2001), pp. 137-162.

[33] J. Norbury, J. Wei, M. Winter, *Existence and Stability of Singular Patterns in a Ginzburg-Landau Equation Coupled with a Mean Field*, Nonlinearity, **15**, No. 6, (2002), pp. 2077-2096.

[34] J. E. Pearson, *Complex Patterns in a Simple System*, Science, **216**, (1993), pp. 189-192.

[35] V. Petrov, S. K. Scott, K. Showalter, *Excitability, Wave Reflection, and Wave Splitting in a Cubic Autocatalysis Reaction-Diffusion System*, Phil. Trans. Roy. Soc. London, Series A, **347**, (1994), pp. 631-642.

[36] W. N. Reynolds, S. Ponce-Dawson, J. E. Pearson, *Dynamics of Self-Replicating Patterns in Reaction-Diffusion Systems*, Phys. Rev. Lett., **72**, (1994), pp. 2797-2800.

[37] W. N. Reynolds, S. Ponce-Dawson, J. E. Pearson, *Dynamics of Self-Replicating Spots in Reaction-Diffusion Systems*, Phys. Rev. E, **56**, No. 1, (1997), pp. 185-198.

[38] H. Riecke, W. J. Rappel, *Coexisting Pulses in a Model for Binary-Mixture Convection*, Phys. Rev. Lett., **75**, (1995), pp. 4035-4038.

[39] W. Sun, T. Tang, M. J. Ward, J. Wei, *Numerical Challenges for Resolving Spike Dynamics for Two Reaction-Diffusion Systems*, to appear, Studies in Appl. Math., (2003).

[40] D. Ueyama, *Dynamics of Self-Replicating Patterns in the One-Dimensional Gray-Scott Model*, Hokkaido Math J., **28**, No. 1, (1999), pp. 175-210.

[41] M. J. Ward, J. Wei, *Hopf Bifurcations and Oscillatory Instabilities of Spike Solutions for the One-Dimensional Gierer-Meinhardt Model*, Journal of Nonlinear Science, Vol. 13, No. 2, (2003), pp. 209-264.

[42] J. Wei, *On Single Interior Spike Solutions for the Gierer-Meinhardt System: Uniqueness and Stability Estimates*, Europ. J. Appl. Math., Vol. **10**, No. 4, (1999), pp. 353-378.

[43] J. Wei, M. Winter, *On a Cubic-Quintic Ginzburg-Landau Equation with Global Coupling*, Proc. Amer. Math. Soc., to appear, (2004).